Journal of Biomolecular Structure and Dynamics

ISSN: 0739-1102 (Print) 1538-0254 (Online) Journal homepage: www.tandfonline.com/journals/tbsd20

Synthesis, anticholinesterase activity and molecular modeling studies of novel carvacrol-substituted amide derivatives

Belma Zengin Kurt, Serdar Durdagi, Gulsen Celebi, Ramin Ekhteiari Salmas & Fatih Sonmez

To cite this article: Belma Zengin Kurt, Serdar Durdagi, Gulsen Celebi, Ramin Ekhteiari Salmas & Fatih Sonmez (2020) Synthesis, anticholinesterase activity and molecular modeling studies of novel carvacrol-substituted amide derivatives, Journal of Biomolecular Structure and Dynamics, 38:3, 841-859, DOI: 10.1080/07391102.2019.1590243

To link to this article: https://doi.org/10.1080/07391102.2019.1590243

JOURNAL OF BIOMOLECULAR STRUCTURE AND DYNAMICS
2020, VOL. 38, NO. 3, 841–859
https://doi.org/10.1080/07391102.2019.1590243

Synthesis, anticholinesterase activity and molecular modeling studies of novel carvacrol-substituted amide derivatives

Belma Zengin Kurt[a], Serdar Durdagi[b], Gulsen Celebi[c], Ramin Ekhteiari Salmas[b] and Fatih Sonmez[d]

[a]Department of Pharmaceutical Chemistry, Faculty of Pharmacy, Bezmialem Vakif University, Istanbul, Turkey; [b]Computational Biology and Molecular Simulations Laboratory, Department of Biophysics, School of Medicine, Bahcesehir University, Istanbul, Turkey; [c]Department of Pharmacology, Faculty of Medicine, Kocaeli University, Kocaeli, Turkey; [d]Pamukova Vocational High School, Sakarya University of Applied Sciences, Sakarya, Turkey

Communicated by Ramaswamy H. Sarma

ABSTRACT

In the present study, 23 novel carvacrol derivatives involving the amide moiety as a linker between the alkyl chains and/or the heterocycle nucleus were synthesized and tested *in vitro* as acetylcholinesterase (AChE) and butyrylcholinesterase (BuChE) inhibitors. 2-(5-Isopropyl-2-methylphenoxy)-*N*-(quinolin-8-yl)acetamide (**5v**) revealed the highest inhibition properties against AChE and BuChE with the IC_{50} values of 1.93 and 0.05 μM, respectively. The blood–brain barrier (BBB) permeability of the potent inhibitor (**5v**) was also assessed by the widely used parallel artificial membrane permeability assay (PAMPA-BBB). The results showed that **5v** is capable of crossing the BBB. Pharmacokinetic and toxicity profiles of the studied molecule predictions were investigated by MetaCore/MetaDrug comprehensive systems biology analysis suite. Bioactive conformations of the synthesized molecules, their predicted binding energies as well as structural and dynamical profiles of molecules at the binding pockets of AChE and BuChE targets were also investigated using different docking algorithms and molecular dynamics (MD) simulations.

Abbreviations: AChE: acetylcholinesterase; BBB: blood–brain barrier; BuChE: butyrylcholinesterase; MD: molecular dynamics; PAMPA: parallel artificial membrane permeability assay

ARTICLE HISTORY
Received 4 February 2019
Accepted 27 February 2019

KEYWORDS
Acetylcholinesterase; Alzheimer's disease; butyrylcholinesterase; carvacrol; molecular docking; molecular dynamics (MD) simulations

1. Introduction

Alzheimer's disease (AD), known as the most common cause of dementia, is a deadly and age-related neurodegenerative disease that affects almost 50 million people in the world and worsens with severe behavioural and psychiatric symptoms in the long run (Wang et al., 2014; Wu et al., 2017). This disease is progressive and irreversible, with the symptoms of memory loss, a decline in language skills, behavioural disturbances and much other cognitive impairment (Li et al., 2017; Tommonaro et al., 2016). The exact etiology of AD remains unknown, but many factors such as β-amyloid (Aβ) deposits, tau protein (τ) aggregation and oxidative stress, decreased level of acetylcholine (ACh), neuroinflammation and dyshomeostasis of biometal are thought to play significant roles in the pathogenesis of the disease (Guzior et al., 2015; Li et al., 2017; Xia et al., 2017). Although numerous therapeutic approaches have been reported, only non-competitive *N*-methyl-D-aspartate (NMDA) receptor antagonist memantine and acetylcholinesterase (AChE) inhibitors, donepezil, rivastigmine, tacrin and galantamine, have been approved by the FDA (Estrada et al., 2016; Sağlık, Ilgın, & Özkay, 2016).

Many studies have been carried out in recent years in order to develop new hit molecules against AD targets in both *in silico* and experimental studies conducted in academia and industry. (Ambure et al., 2018; Dutta & Mattaparthi, 2018; Ferreira Neto et al., 2018; Iqbal, Anantha Krishnan, & Gunasekaran, 2018; Shiri, Pirhadi, & Ghasemi, 2018). Most of the drugs used in AD are aimed at preventing the decrease of ACh level. According to the cholinergic hypothesis, the cognitive deficits in AD are related with correlation deficits such as cholinergic-reduced choline acetyltransferase (ChAT) activity and synaptic ACh synthesis. The main purpose here is to increase the ACh level in the synaptic cleft by the inhibition of cholinesterases (Liu, Fang, Zhang, Gou, & Chen, 2017; Maryamabadi, Hasaninejad, Nowrouzi, & Mohebbi, 2017; Wang et al., 2017). There are two types of cholinesterases in the body, AChE (EC 3.1.1.7) and butyrylcholinesterase (BuChE; EC 3.1.1.8). AChE as a key enzyme target is not only used in enhancing cholinergic transmission in the synaptic cleft but also can be used in reducing the aggregation of amyloid-beta (Aβ) peptide and in the hydrolysis of ACh which causes neurotoxic fibril formation in AD (Guzior et al., 2015; Kurt et al., 2017). BuChE is

CONTACT Serdar Durdagi serdar.durdagi@med.bau.edu.tr; Belma Zengin Kurt BZengin@bezmialem.edu.tr
Supplemental data for this article can be accessed online at https://doi.org/10.1080/07391102.2019.1590243

another enzyme which is expressed in selected areas of the central and peripheral nervous systems and also capable of hydrolysing ACh (Eghtedari et al., 2017; Panek et al., 2017). The similarity between the amino acid sequence of AChE and BuChE is very high (almost 84%), so the answers they provide are matching (Chen et al., 2017). Although AChE inhibitors (AChEI) in AD show beneficial palliative properties, cholinergic drugs have not shown much efficacy to prevent disease progression. Currently, there is no effective therapy to treat, stop or even slow down the progression of the disease, and therefore the discovery of effective novel therapeutics is needed (León, Garcia, & Marco-Contelles, 2013).

Carvacrol is the main component of the monoterpenes found as essential oils in *Thymus vulgaris* (Majdi, Malekzadeh-Mashhady, Maroufi, A, & Crocoll, 2017; Sow, Tirtawinata, Yang, Shao, & Wang, 2017) Carvacrol is an important small therapeutic molecule because of its antioxidative, antimicrobial, antitussive and antibacterial properties (Höferl et al., 2009; Rodríguez, Ortuño, Benedito, & Bon, 2013). Apart from these, carvacrol has also been reported to reveal anti-inflammatory, immunomodulatory and chemopreventive properties (Hussein et al., 2017). Carvacrol demonstrates the potential protective effect on central nervous system (CNS) diseases through various mechanisms. These properties have important role on antidepressant effect, anxiolytic effect and AChE activity (Dati et al., 2017; López et al., 2015; Zhong et al., 2013). In addition, amidic or imidic substituents are important functional groups forming hydrogen bonds in the catalytic domain of human AChE (Kurt, Gazioglu, Sonmez, & Kucukislamoglu, 2015; Mohamed, Osman, Tin, & Rao, 2013; Sonmez et al., 2017).

Besides of these reported evidences, a good penetration across the *blood–brain barrier* (BBB) is a desired condition for the CNS drugs, and it is known that the BBB allows the diffusion of hydrophobic and small polar molecules, whereas it cuts down large or hydrophilic molecules into the blood and cerebrospinal fluid (Pérez-Areales et al., 2014). Although many synthetic AChEIs and BuChEIs have been reported in the last decades, there is still limited study on the natural products and their derivatives having high BBB permeability as the ChEIs. Therefore, the main goal of this present study is the synthesis of effective AChEIs and BuChEIs including natural compounds, to investigate their BBB permeability and also to determine their inhibition mechanism and structure–activity relationships (SARs) as a continuation of our interest in AChEIs and BuChEIs.

Based on the above consideration, we hypothesized that carvacrol is a small polar natural compound and can easily penetrate across the BBB; however, it has low inhibitory activity against ChEs, and so the presence of amide moiety could contribute to the inhibitory activity of carvacrol. Therefore, in the present study, 23 novel carvacrol (**5a**-**w**) derivatives substituted with aliphatic and aromatic amide derivatives were synthesized and their inhibitory effects on AChE and BuChE were evaluated. Also, the BBB permeability of the novel compounds has been assessed by the widely used parallel artificial membrane permeability assay (PAMPA-BBB). Moreover, molecular modeling studies were also applied. Molecular docking studies were carried out to clarify the inhibition mode for the studied compounds at the active sites of the target structures. Binding poses and binding energies of studied compounds at the binding pockets of AChE and BuChE targets were determined. Predicted binding energies of these compounds and structural and dynamical profiles of molecules at the target sites were estimated using different docking algorithms (i.e. induced fit docking (IFD), quantum polarized ligand docking (QPLD) and GOLD) as well as molecular dynamics (MD) simulations and post-processing MD analysis. Moreover, the studied compounds were put through further investigation regarding their pharmacokinetic and toxicity properties using MetaCore/MetaDrug comprehensive systems biology analysis suite using binary disease and toxicity QSAR models.

2. Results and discussion

Although the pathogenesis of AD has not been fully clarified, one of the most important theories is the decreased levels of ACh and butyrylcholine which is observed in the brains of patients with AD. Thus, the inhibition of AChE and BuChE enzymes that hydrolyse ACh and BCh neurotransmitters can be considered as therapeutic approach. For this reason, many research groups have conducted investigations of the inhibitory activity for these enzymes involved in AD pathogenesis (Cavdar et al., 2019; Gao, Tang, Liu, & Liu, 2019; Pascoini et al., 2019; Zilbeyaz, Stellenboom, Güney, Oztekin, & Senturk, 2018). In this study, 23 novel carvacrol derivatives involving the amide moiety as a linker between the alkyl chains and/or the heterocycle nucleus were synthesized and tested *in vitro* as AChE and BuChE inhibitors.

2.1. Chemistry

The synthesis of the target carvacrol derivatives (**5a-w**) was accomplished in four steps (Scheme 1). The ethyl 2-(5-isopropyl-2-methylphenoxy)acetate (**2**) was synthesized from the carvacrol (**1**) by a nucleophilic substitution. **2** was hydrolysed with 10% NaOH (aq) to give 2-(5-isopropyl-2-methylphenoxy) acetic acid (**3**) and then **3** was chlorinated with $SOCl_2$. In the last step, 2-(5-isopropyl-2-methylphenoxy)acetyl chloride (**4**) was reacted with aliphatic or aromatic amine derivatives. **5a-w** were obtained in acceptable yields ranging from 40 to 86%. All the novel compounds were characterized by ^{1}H NMR, ^{13}C NMR, IR, MS and elemental analyses.

2.2. Cholinesterase inhibitory activity

The inhibitory activities of the synthesized compounds (**5a-w**) on AChE and BuChE were determined by Ellman's method (Ellman, Courtney, Andres, & Featherstone, 1961). The IC_{50} values for AChE and BuChE inhibitions are summarized in Table 1. The IC_{50} values against AChE and BuChE ranged from 1.93 to $>200\,\mu M$ and from 0.05 to 184.50 μM, respectively.

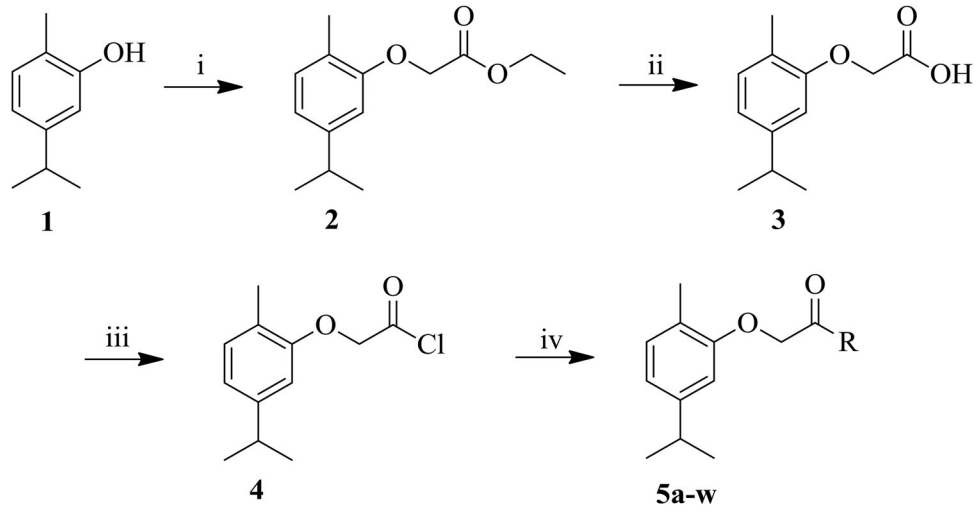

Scheme 1. Synthesis of new carvacrol-substituted amide derivatives. Reaction conditions: (i) Ethylbromoacetate, K_2CO_3, Acetone, reflux, 5 h; (ii) 10% NaOH (aq), reflux, 6 h; (iii) $SOCl_2$, 80 °C, 2h; (iv) Amine derivatives, Et_3N, CH_2Cl_2, 60 °C, overnight.

The majority of the synthesized carvacrol-substituted amide derivatives revealed significantly higher inhibition activity than carvacrol against AChE. Similarly, all of the synthesized compounds have higher BuChE inhibitory activity than carvacrol. Among them, **5v** exhibited the strongest inhibition against AChE with an IC_{50} value of 1.93 μM, which is 149-fold more than that of carvacrol (IC_{50} = 288.26 μM), and it showed similar activity with the galantamine, used as a standard (IC_{50} = 2.21 μM), while it represented less inhibitory activity than donepezil (IC_{50} = 0.03 μM) and tacrine (IC_{50} = 0.17 μM), which are well known as AChE inhibitors. Compound **5v** displayed the strongest inhibition against BuChE with an IC_{50} value of 0.05 μM, which is 8216-fold more than that of carvacrol (IC_{50} = 410.79 μM), 372-fold more than that of galantamine (IC_{50} = 18.60 μM) and 52-fold more than that of donepezil (IC_{50} = 2.58 μM) but 2.5-fold less than that of tacrine (IC_{50} = 0.02 μM).

The following SAR observations can be drawn from data of Table 1: (i) in comparison to **5a**-**e** and **5i**, involving alkyl or cyclic alkyl group binding to *N*-atom, an increase in the C number of alkyl chains and the steric hindrance by binding of the second alkyl group on the *-NH* of the amide moiety may lead to a decline in the inhibitory activity against both AChE and BuChE, compare **5a** (having *N*-methyl group, IC_{50} = 20.54 and 21.87 μM for AChE and BuChE, respectively) with **5b** (having *N*-propyl group, IC_{50} = 37.51 and 32.65 μM for AChE and BuChE, respectively), **5e** (having *N*-cyclohexyl group, IC_{50} = 58.28 and 32.89 μM for AChE and BuChE, respectively) and **5i** (having *N*-dihydro-indenyl group, $IC_{50} \geq$ 200 and 45.04 μM for AChE and BuChE, respectively) and (compare **5c** (having *N,N*-diethyl group, IC_{50} = 73.70 and 80.20 μM for AChE and BuChE, respectively) with **5d** (having *N,N*-diisopropyl group, IC_{50} = 95.96 and 96.50 μM for AChE and BuChE, respectively)). (ii) The expansion of the pyrrolidine ring of **5f** (IC_{50} = 144.21 μM) to a piperidine ring (compound **5g**: $IC_{50} \geq$ 200 μM) and morpholine ring (**5h**: IC_{50} = 197.77 μM) decreased the AChE inhibitory activity. These declines in items (i) and (ii) can simply be explained as increasing steric hindrances decreases H-bonding capability of N-atoms. (iii) The presence of an ethyleneamine (-$HNCH_2CH_2$-) group as a spacer between the carbonyl moiety and the pyrrolidine or morpholine ring negatively affected the inhibitory activity against both ChEs (compare **5f** (IC_{50} = 144.21 and 30.31 μM for AChE and BuChE, respectively)) with **5j** ($IC_{50} \geq$ 200 and 74.40 μM for AChE and BuChE, respectively) and (compare **5 h** (IC_{50} = 197.77 and 9.39 μM for AChE and BuChE, respectively)) with **5k** ($IC_{50} \geq$ 200 and 137.38 μM for AChE and BuChE, respectively). (iv) The presence of an amine (-NH) group between the carbonyl moiety and the piperidine or morpholine ring increased the AChE inhibitory activity (compare **5 g** ($IC_{50} \geq$ 200 μM)) with **5q** (IC_{50} = 66.70 μM) and (compare **5 h** (IC_{50} = 197.77 μM)) with **5o** (IC_{50} = 191.56 μM). This enhancement can be linked to the presence of amine group, increasing the possibility of hydrogen bond formation with the amino acid residues in active side. (v) The increase in the electron density of the heterocyclic aromatic moiety (pyridine, pyrimidine and quinoline) and binding amide moiety enhanced the inhibitory activity against both AChE and BuChE targets (compare **5t** (having pyridine, IC_{50} = 92.31 and 184.50 μM for AChE and BuChE, respectively)) with **5 u** (having pyrimidine, IC_{50} = 20.74 and 2.82 μM for AChE and BuChE, respectively) and **5v** (having quinoline, IC_{50} = 1.93 and 0.05 μM for AChE and BuChE, respectively). This is an expected effect because the increase in electron density of heterocyclic aromatic moiety can lead to the formation of π–π stacking or π–cation interactions with the active site amino acids. When the sizes of the molecules are compared to the approved drugs, they have similar sizes (i.e. while donepezil has 28 non-hydrogen atoms, corresponding number is 25 in **5v**), so the ligand efficiency trend can also be interpreted from the inhibitory activity results of studied molecules.

2.3. Molecular docking

Studied molecules were docked into the binding pockets of AChE and BuChE targets using different docking algorithms.

Table 1. *In vitro* inhibition IC_{50} values (μM) and selectivity of compounds **5a-w** for AChE and BuChE.

Compound	Structure	AChE (IC_{50}, μM)[a]	BuChE (IC_{50}, μM)[a]	Selectivity index[b]
Carvacrol[c]	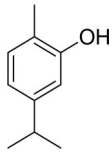	288.26 ± 1.112	410.79 ± 1.238	1.43
5a	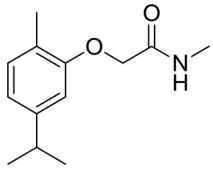	20.54 ± 0.47	21.87 ± 1.51	1.07
5b	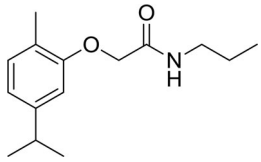	37.51 ± 1.14	32.65 ± 0.98	0.87
5c	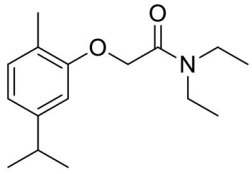	73.70 ± 1.47	80.20 ± 0.98	1.09
5d	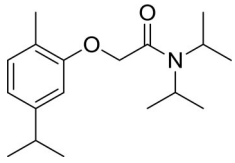	95.96 ± 1.22	96.15 ± 1.21	1.00
5e	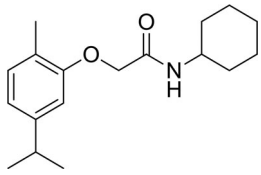	58.28 ± 0.55	37.89 ± 0.68	0.65
5f	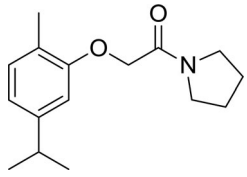	144.21 ± 1.22	30.31 ± 0.78	0.21
5g	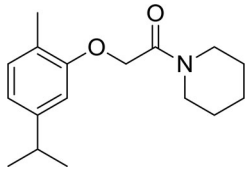	>200	2.72 ± 0.51	<0.01
5h	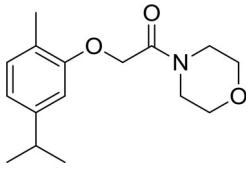	197.77 ± 1.61	9.39 ± 0.26	0.05
5i	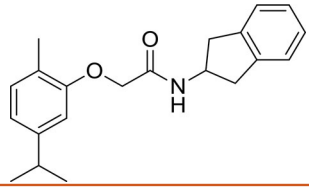	>200	45.04 ± 0.95	<0.23

(*continued*)

Table 1. Continued.

Compound	Structure	AChE (IC_{50}, μM)[a]	BuChE (IC_{50}, μM)[a]	Selectivity index[b]
5j	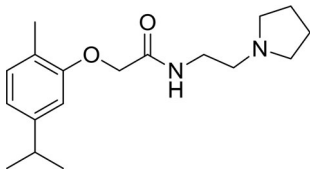	>200	74.40 ± 1.42	<0.37
5k	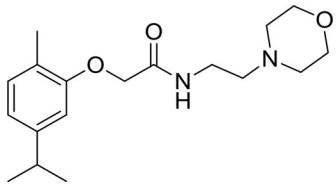	>200	137.38 ± 1.29	<0.69
5l	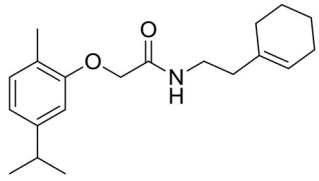	>200	43.16 ± 1.23	<0.22
5m	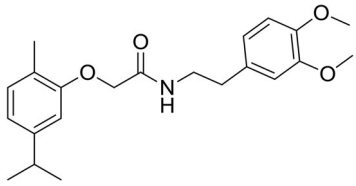	>200	59.56 ± 1.44	<0.30
5n	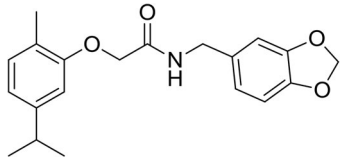	116.69 ± 1.01	2.68 ± 0.38	0.02
5o	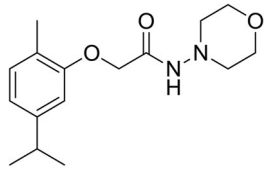	191.56 ± 1.14	140.07 ± 1.33	0.73
5p	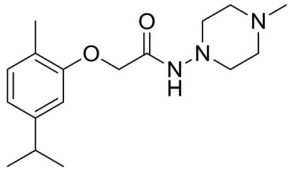	60.11 ± 1.85	3.08 ± 0.63	0.05
5q	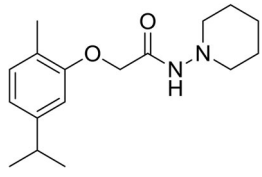	66.70 ± 1.08	61.89 ± 1.27	0.93
5r	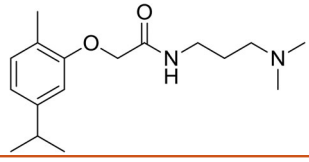	88.68 ± 1.43	44.05 ± 1.51	0.50

(*continued*)

Table 1. Continued.

Compound	Structure	AChE (IC_{50}, μM)[a]	BuChE (IC_{50}, μM)[a]	Selectivity index[b]
5s	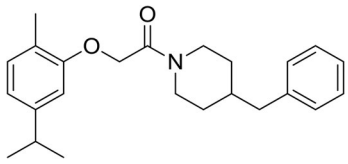	88.28 ± 1.28	30.15 ± 1.66	0.34
5t	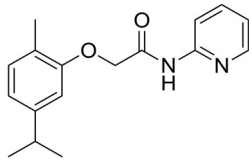	92.31 ± 1.65	184.50 ± 1.73	2.00
5u	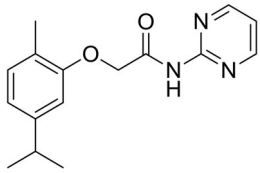	20.74 ± 0.67	2.82 ± 0.66	0.14
5v	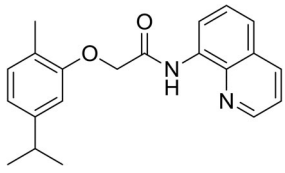	1.93 ± 0.32	0.05 ± 0.07	0.03
5w	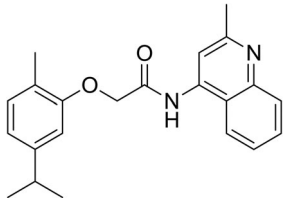	65.61 ± 1.32	37.40 ± 1.14	0.57
Galantamine	–	2.21 ± 0.05	18.60 ± 0.52	15.37
Donepezil[d]	–	0.03 ± 0.0005	2.58 ± 0.65	86.00
Tacrine[e]	–	0.17 ± 0.0119	0.02 ± 0.004	0.12

[a]IC_{50} values represent the means ± SEM of three parallel measurements ($p < 0.05$).
[b]Selectivity index = IC50 (BuChE) / IC50 (AChE).
[c]From Kurt et al., 2017
[d]From Li et al., 2017
[e]From Muñoz-Ruiz et al., 2005

Table 2 represents GOLD Fitness and ChemScore results of studied compounds at the binding cavities of AChE and BuChE. Docking results were compared with known inhibitors donepezil, galantamine and tacrine. Docking results show that while standard inhibitors have better GoldFitness and ChemScore values than studied molecules at the binding pocket of AChE, corresponding results were similar for BuChE. Docking scores of studied molecules and known inhibitors using other docking programs were represented and are compared to each other in Figure 1. Detailed results are provided in Table S1 (Supporting Materials). All used docking programs predicted the donepezil as the tightest binder molecule which fits well with the experimental results. Because of the limitations on the basis of docking algorithm, it is not expected to get absolute binding affinity values obtained from *in vitro* results. However, when the studied molecules are divided into the weak, moderate and strong binders, it can be seen that experimental results and especially Glide/IFD results fit well to each other. Thus, for further analysis (i.e. MD simulations), initial structures were used from top-docking poses derived from Glide/IFD algorithm.

2.4. MD simulations

In order to evaluate the dynamics of the selected ligands (**5v** and **5w**) and also fluctuations of the protein backbones in both ligand-bound and ligand-free (*apo*) systems, the complexes obtained from the docking simulations (Figure S1, supplementary material) were submitted into all-atom MD simulations. The results were monitored throughout the MD simulations as the root-mean-square deviation (RMSD) of the atomic positions with respect to the initial conformers (Figure 2).

The calculations were performed based on two different approaches, '*ProFit*' and '*Lig Fit*', which, respectively, show

Table 2. (Top) GOLD Fitness and ChemScore results of studied compounds at the binding cavities of AChE and BuChE; (bottom) GOLD Fitness and ChemScore results of known approved compounds at the binding cavities of AChE and BuChE.

	AChE				BuChE			
Comp.	GoldScore Fitness Min.	GoldScore Fitness Max.	Average	ChemScore (kcal/mol)	GoldScore Fitness Min.	GoldScore Fitness Max.	Average	ChemScore (kcal/mol)
5a	51.55	65.19	59.22 ± 2.64	−10.35	36.45	44.00	39.78 ± 2.10	−11.19
5b	59.73	69.86	66.26 ± 2.33	−10.22	42.47	50.25	46.84 ± 1.59	−10.92
5c	53.24	64.85	59.98 ± 2.36	−12.51	39.24	46.86	43.65 ± 1.87	−11.23
5d	29.68	65.99	50.76 ± 7.62	−10.51	41.93	51.46	47.67 ± 2.42	−9.57
5e	62.64	73.15	68.61 ± 1.85	−12.88	49.14	57.04	54.69 ± 1.93	−10.92
5f	52.68	65.60	60.82 ± 2.40	−11.52	42.90	46.63	45.01 ± 1.00	−9.12
5g	48.53	67.21	58.30 ± 3.49	−12.40	40.79	47.49	45.62 ± 1.98	−11.19
5h	51.13	66.77	60.53 ± 3.35	−10.82	38.04	48.21	44.94 ± 1.57	−10.08
5i	68.53	80.77	73.58 ± 3.03	−12.81	48.35	58.01	53.60 ± 1.95	−11.37
5j	69.62	79.98	74.33 ± 2.57	−11.10	48.05	58.60	53.25 ± 2.55	−13.01
5k	65.32	79.95	74.56 ± 3.18	−11.69	48.18	58.77	53.82 ± 1.88	−11.26
5l	69.73	83.61	77.53 ± 3.14	−12.95	50.32	63.31	55.83 ± 3.08)	−12.95
5m	74.36	88.21	81.60 ± 3.27	−12.74	48.89	62.79	56.54 ± 3.13	−10.68
5n	66.92	86.40	78.83 ± 3.69	−10.60	48.72	62.17	54.15 ± 3.36	−10.60
5o	60.73	68.63	64.98 ± 2.27	−11.47	44.63	54.11	49.01 ± 2.20	−11.07
5p	60.36	73.37	68.09 ± 3.03	−11.96	44.87	52.96	49.11 ± 2.05	−11.15
5q	59.19	68.98	68.71 ± 2.27	−11.76	45.15	57.51	51.96 ± 2.85	−6.89
5r	73.17	89.75	84.32 ± 3.57	−11.26	54.29	68.73	61.21 ± 2.64	−6.05
5s	60.71	76.94	69.34 ± 4.18	−13.79	49.15	59.75	56.49 ± 2.53	−9.54
5t	63.30	76.56	70.48 ± 3.20	−10.53	44.79	55.35	51.80 ± 2.73	−6.34
5u	61.23	76.40	70.45 ± 3.56	−10.48	43.79	54.09	50.47 ± 2.26	−6.32
5v	66.40	79.73	72.08 ± 3.24	−11.04	52.81	65.06	59.36 ± 3.18	−8.24
5w	66.48	77.60	72.72 ± 3.18	−13.36	48.98	60.41	55.47 ± 3.45	−7.57

Comp.	AChE			BuChE		
	GoldScore Fitness (top)	Average Score	ChemScore (top) (kcal/mol)	GoldScore Fitness (top)	Average Score	ChemScore (top) (kcal/mol)
Donepezil	94.31	86.53 ± 5.16	−14.90	64.63	56.04 ± 2.88	−7.49
Galantamine	84.64	79.96 ± 1.98	−11.19	51.04	46.57 ± 0.60	−6.98
Tacrine	83.70	82.43 ± 1.15	−13.80	47.65	47.11 ± 1.79	−7.07

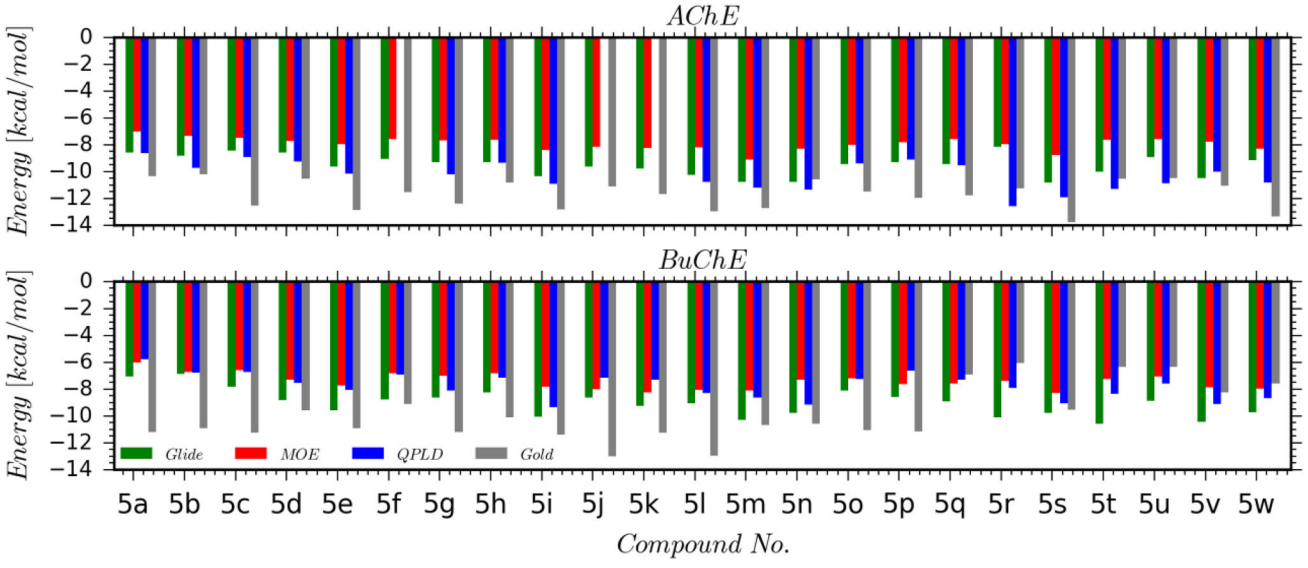

Figure 1. Glide/IFD, MOE/IFD, QPLD and Gold (ChemScore) results of studied compounds at the binding cavities of AChE (top) and BuChE (bottom). Docking scores are in kcal/mol.

the dynamics of the systems when the trajectory frames were fitted based on the protein (i.e. translational) and ligand atoms (i.e. rotational), respectively. It provides better understanding of translational and rotational dynamics of studied ligands at the binding cavity of targets through the MD simulations. The average values of RMSD were calculated for the individual systems, helping compare the fluctuations of the systems, as shown in Figure 2. The results are in consistent with the experimental data. The apo conformer, which is free of ligand, revealed less structural stability in comparison with the ligand-bound systems.

In the case of the ligand-bound systems, the ProFit RMSD average values for the **5v** and **5w** were calculated to be 4.84 and 5.60 Å, respectively, which demonstrate that compound **5v** seems slightly more stable with lower diffusion than compound **5w**. Also, **5v** showed smaller rotational changes in

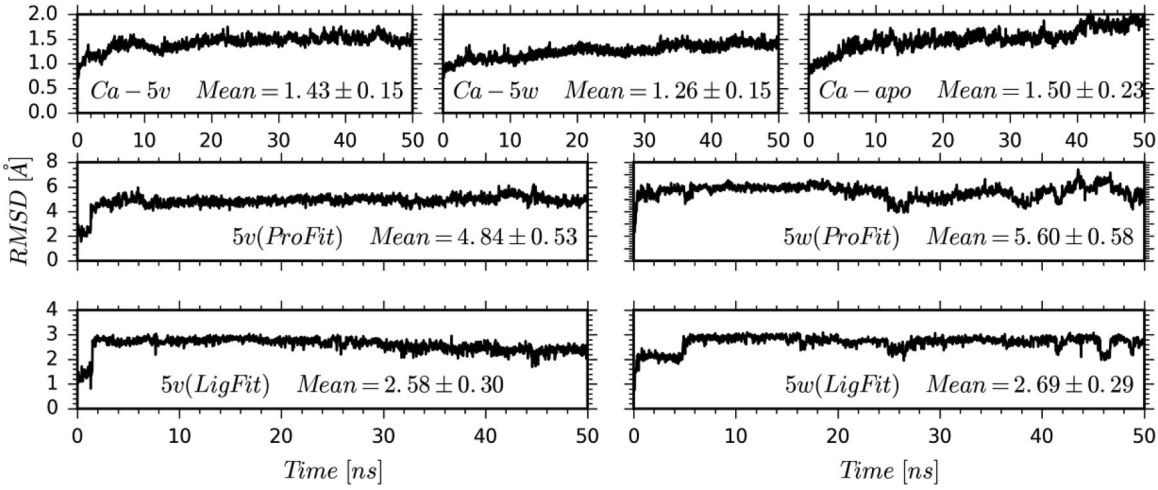

Figure 2. ProFit and LigFit RMSD analysis of compounds **5v** and **5w** throughout MD simulations. (ProFit shows the RMSD of a ligand when the protein–ligand complex is first aligned on the protein backbone of the reference and then the RMSD of the ligand heavy atoms is measured. If the values observed are significantly larger than the RMSD of the protein, then it is likely that the ligand has diffused away from its initial binding site. LigFit shows the RMSD of a ligand that is aligned and measured just on its reference conformation. This RMSD value measures the internal fluctuations of the ligand atoms.)

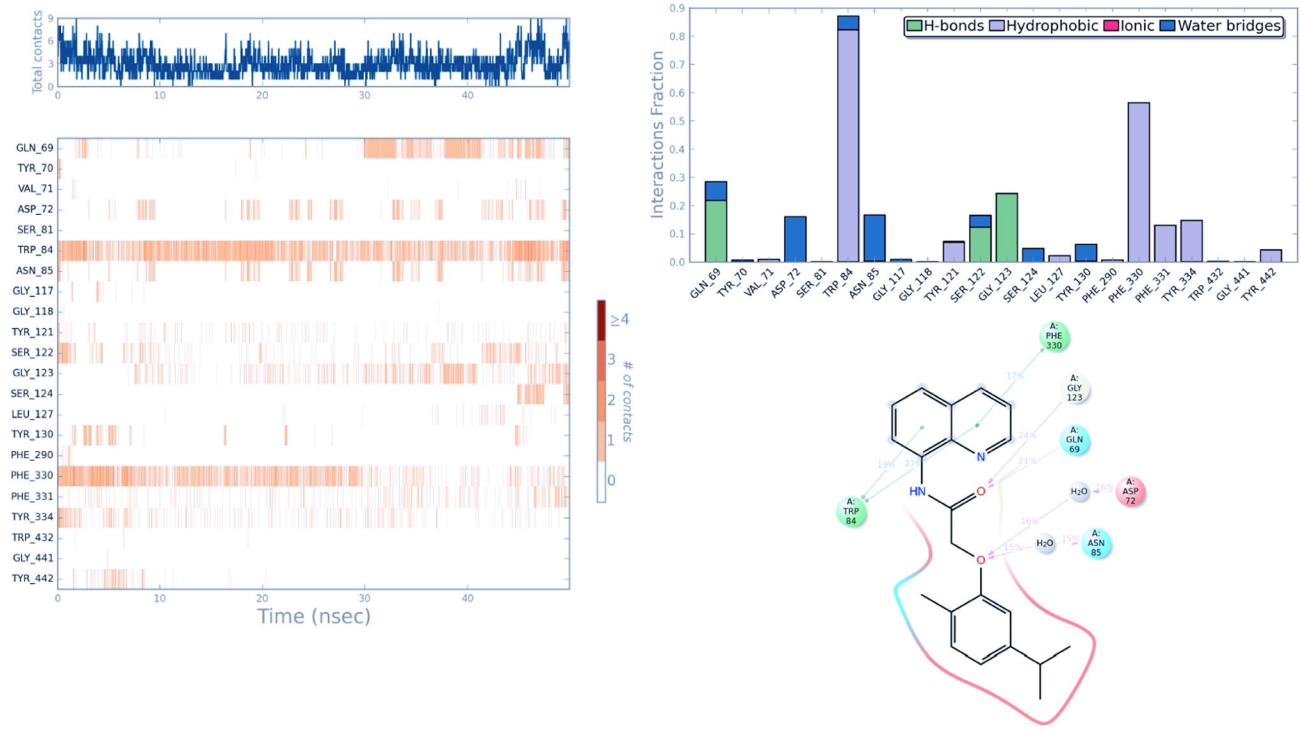

Figure 3. (left) A timeline representation of the interactions and contacts of compound **5v** at the binding pocket of AChE throughout MD simulations. (right) Interaction fractions of residues are shown by the stacked bar charts which are normalized over the course of the trajectory frames. Interactions that occur more than 15% of the simulation time throughout 50-ns MD simulations are also shown. Residue numbers are based on the sequence numbering in the used PDB structure.

the cavity. The observed data can be linked to strongly formed chemical interactions of **5v** within the active site amino acids.

In addition, interactions of studied molecules with the active site residues were monitored throughout the simulations (Figures 3 and 4). These contacts between ligand and target residues were categorized into four different types (i.e. hydrogen bonding, hydrophobic, ionic and water-bridge) and represented as stacked bar charts which are normalized over the course of the trajectories. These figures also assist for monitoring to see the changes of constructing chemical bonding interactions from the beginning of simulations (i.e. input coordinates from docking) throughout the simulations. Moreover, conformational evolution of rotatable bonds in the **5v** and **5w** was analysed throughout the simulation (Figures 5 and 6). Each rotatable bond torsion is accompanied by a radial plot and bar plot. While radial plots describe the change of the dihedral angle during the simulation (i.e. beginning of the simulation is in the centre of the plot and the time evolution is plotted radially outwards), the bar plots summarize the data on the radial plots by showing the probability density of the torsion. The rotatable bonds in **5v** seem more stable than those in **5w**, in which wide spectrum of torsional angles appeared – as it is mentioned in the

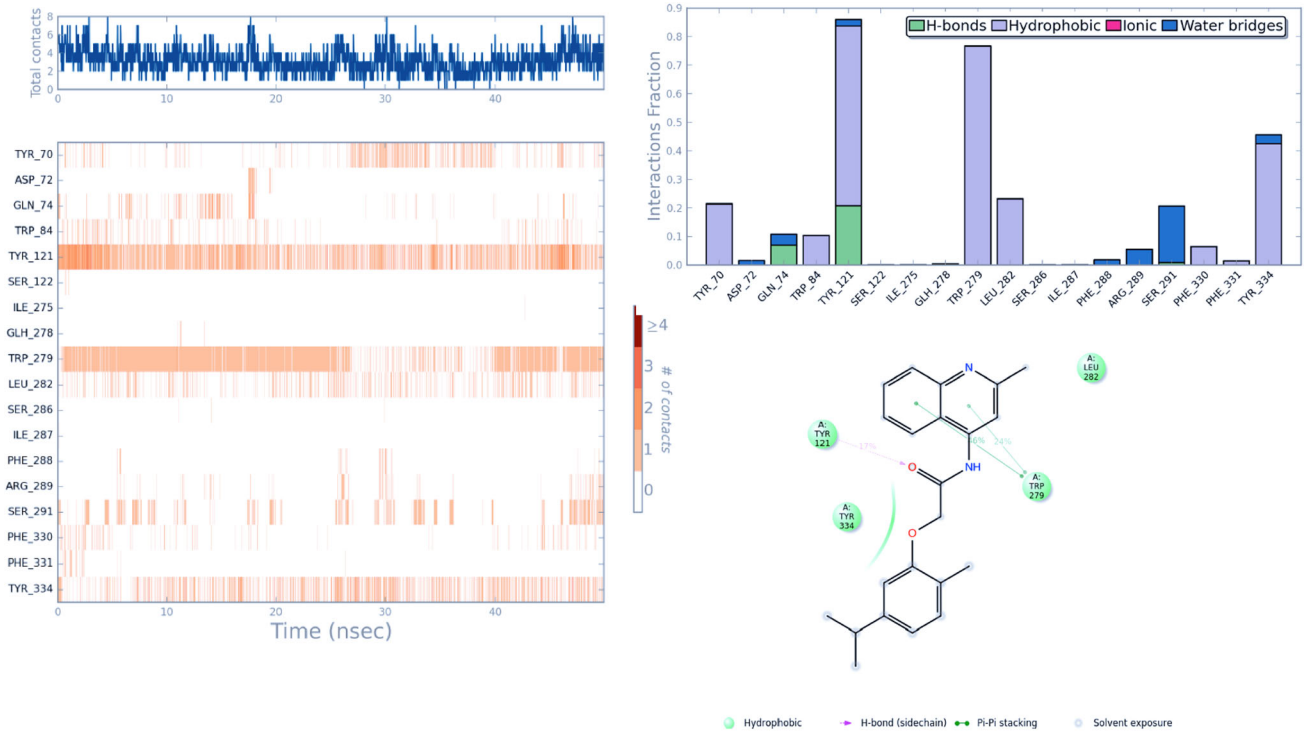

Figure 4. (Left) A timeline representation of the interactions and contacts of compound **5w** at the binding pocket of AChE throughout MD simulations. (Right) Interaction fractions of residues are shown by the stacked bar charts which are normalized over the course of the trajectory frames. Interactions that occur more than 15% of the simulation time throughout 50-ns MD simulations are also shown. Residue numbers are based on the sequence numbering in the used PDB structure.

RMSD analysis, the structural stability of the ligand can be due to the interactions established in the binding site.

When top-docking poses and ligand-binding pocket residue interactions throughout the MD simulations were compared, it can be seen that ligands change their initial position (RMSD is about 5 Å) during the simulations in order to construct more strong new interactions.

It must be noted that MD simulations of known inhibitor donepezil at the binding pocket of AChE represent similar crucial residues (i.e. Trp84, Trp279, Tyr334) which is also found to be important for inhibitor binding with the studied molecules (Figure S2, Supporting Information).

2.5. Ligand binding domain analysis

Interestingly, in comparison between **5v** (having quinoline) and **5w** (having 2-methyl-quinoline), the presence of methyl group and binding position (**5v** bound from C_8 to amide moiety, while **5w** bound from C_4) of heterocyclic ring significantly decreased inhibitory activity against both ChEs. To understand this decline, the structural and dynamical profiles of these molecules at the target sites were estimated using docking and MD simulation methods. According to MD results (Figures 2–6), compound **5v** at the AChE revealed high affinity towards Trp84 and Phe330 by forming mainly π–π stacking interactions and Gln69, Ser122 and Gly123 via hydrogen bonding interactions. On the other hand, Tyr121 and Trp279 residues form strong interactions with the compound **5w** at the binding site of the enzyme. The hydrophobic interactions were also observed for Tyr70, Trp84, Leu282 and Tyr334 with compound **5w**. Furthermore, Tyr121 engaged in a hydrogen bond interaction with the carbonyl oxygen of the compound **5w**.

2.6. MetaCore/MetaDrug analysis

The studied molecules were investigated for their pharmacokinetic and toxicity properties using MetaCore/MetaDrug comprehensive systems biology analysis suite with the help of available absorption, distribution, metabolism and excretion (ADME), disease and toxicity QSAR models. Table 3 compares predicted pharmacokinetic profiles of **5v** and **5w** with approved drugs rivastigmine, tacrine and donepezil. Results show that both molecules permeate the BBB. The compounds show high lipophilicity and moderate human serum protein binding profiles and do not block the human ether a-go-go-related gene (hERG) channel (Table 3). Toxicity properties of **5v** and **5w** were studied with 26 different toxicity QSAR models (Table 4). Both the compounds **5v** and **5w** did not show any high toxicity risks. Slight toxicity risk appeared only in one property (epididymis) for **5w** (the predicted value (0.51) was very close to cutoff (0.50)). It must be noted that while none of the toxicity QSAR models show **5v** as toxic, toxicity predicted only in one model for **5w**. Corresponding toxicity results appeared in three models (i.e. cardiotoxicity, genotoxicity and liver cholestasis) for rivastigmine, in nineteen models for tacrine and in four models for donepezil.

2.7. In vitro BBB permeability using PAMPA-BBB

A good penetration across the *BBB* is desired condition for the CNS drugs (Pérez-Areales et al., 2014). Brain

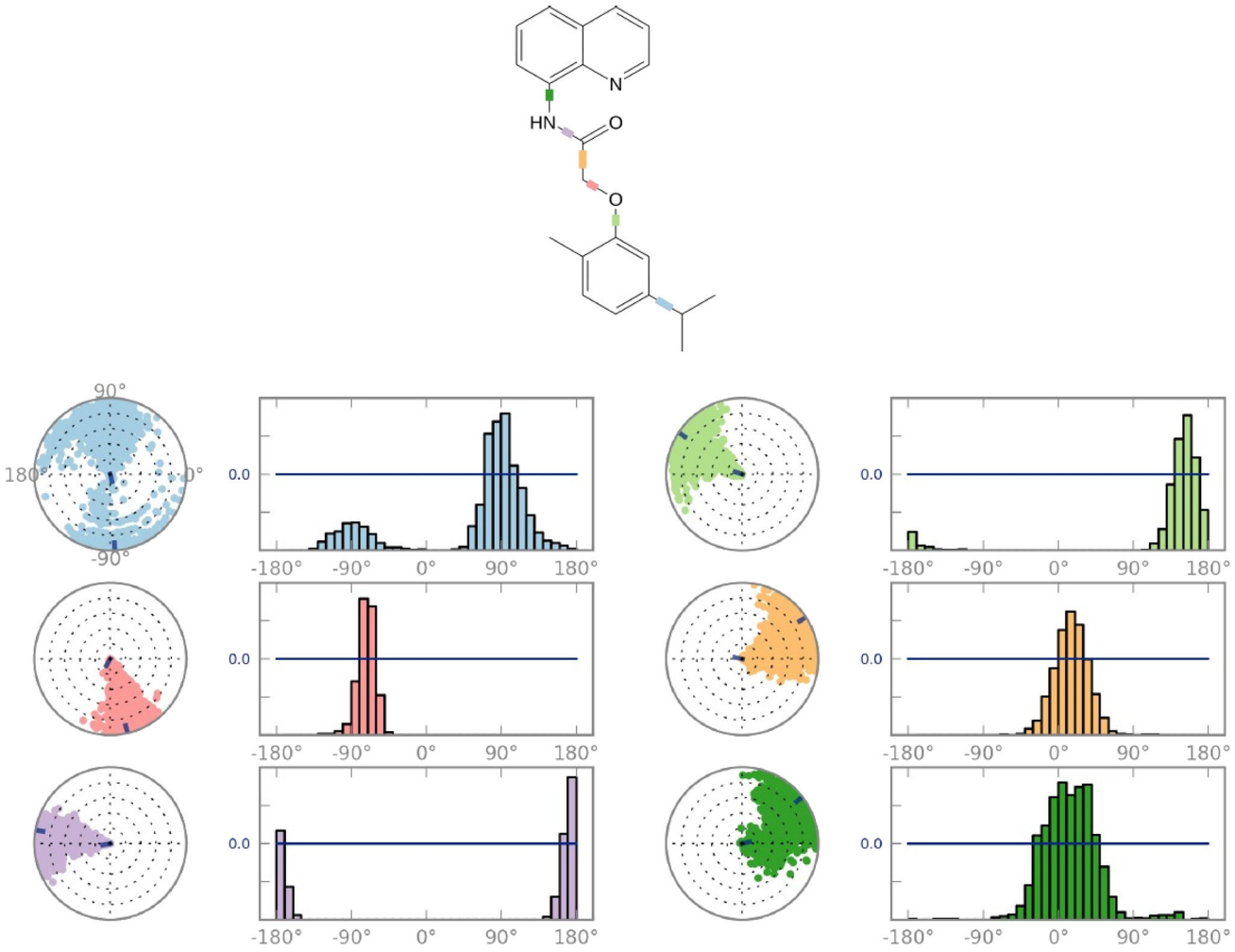

Figure 5. Torsional analysis of **5v** throughout MD simulations. (The ligand torsion plot summarizes the conformational evolution of every rotatable bond in the ligand throughout the simulation trajectory. The top panel shows the 2D schematic of a ligand with color-coded rotatable bonds. Each rotatable bond torsion is accompanied by a dial plot and bar plots of the same colour.)

permeations of **5v**, the most potent compound in this study, and the well-known AChE inhibitors (tacrine, donepezil and rivastigmine) were determined through the parallel artificial membrane permeation assay (PAMPA), described by Di, Kerns, Fan, McConnell, and Carter (2003). This assay involved measuring the rate at which a compound passively diffuses across the lipid barrier separating a donor compartment and an acceptor compartment filled with phosphate buffer (pH 7.4). The concentrations of the compound in both compartments were then measured to obtain the effective permeability rate (P_e). It has been established that compounds with the P_e values above 4×10^{-6} cm s^{-1} penetrate into CNS easily (CNS+), while compounds with the P_e value below 2×10^{-6} cm s^{-1} do not (CNS−). In hybrids having the permeability values between these boundary limits, it is difficult to estimate whether they cross BBB or not (CNS +/−) (Nepovimova et al., 2015). **5v** (P_e = 4.38×10^{-6} cm s^{-1}) showed greater permeability values than that limit, pointing out that these molecules would cross the BBB by passive diffusion (Table 5). Donepezil (P_e = 6.80×10^{-6} cm s^{-1}) and rivastigmine (P_e = 5.78×10^{-6} cm s^{-1}) showed a higher P_e than **5v**, while the P_e of tacrine (P_e = 4.51×10^{-6} cm s^{-1}) and **5v** were fairly close.

3. Conclusions

A series of 23 novel carvacrol-substituted amide moiety as a linker between the alkyl chains and/or the heterocycle nucleus were synthesized and their inhibitory activities on AChE and BuChE were evaluated. Among them, **5v** showed the strongest inhibition against AChE and BuChE with IC_{50} values of 1.93 μM, which is 149-fold more than that of carvacrol (IC_{50} = 288.26 μM), and it showed similar activity with the galantamine, used as a standard (IC_{50} = 2.21 μM). Compound **5v** also exhibited the strongest inhibition against BuChE with an IC_{50} value of 0.05 μM, which is 8216-fold more than that of carvacrol (IC_{50} = 410.79 μM), 372-fold more than that of galantamine (IC_{50} = 18.60 μM) and 52-fold more than that of donepezil (IC_{50} = 2.58 μM). Molecular modeling approaches, including docking and MD simulation methods, suggested that both compounds **5v** and **5w** were conformationally stable inside the binding cavity, which is

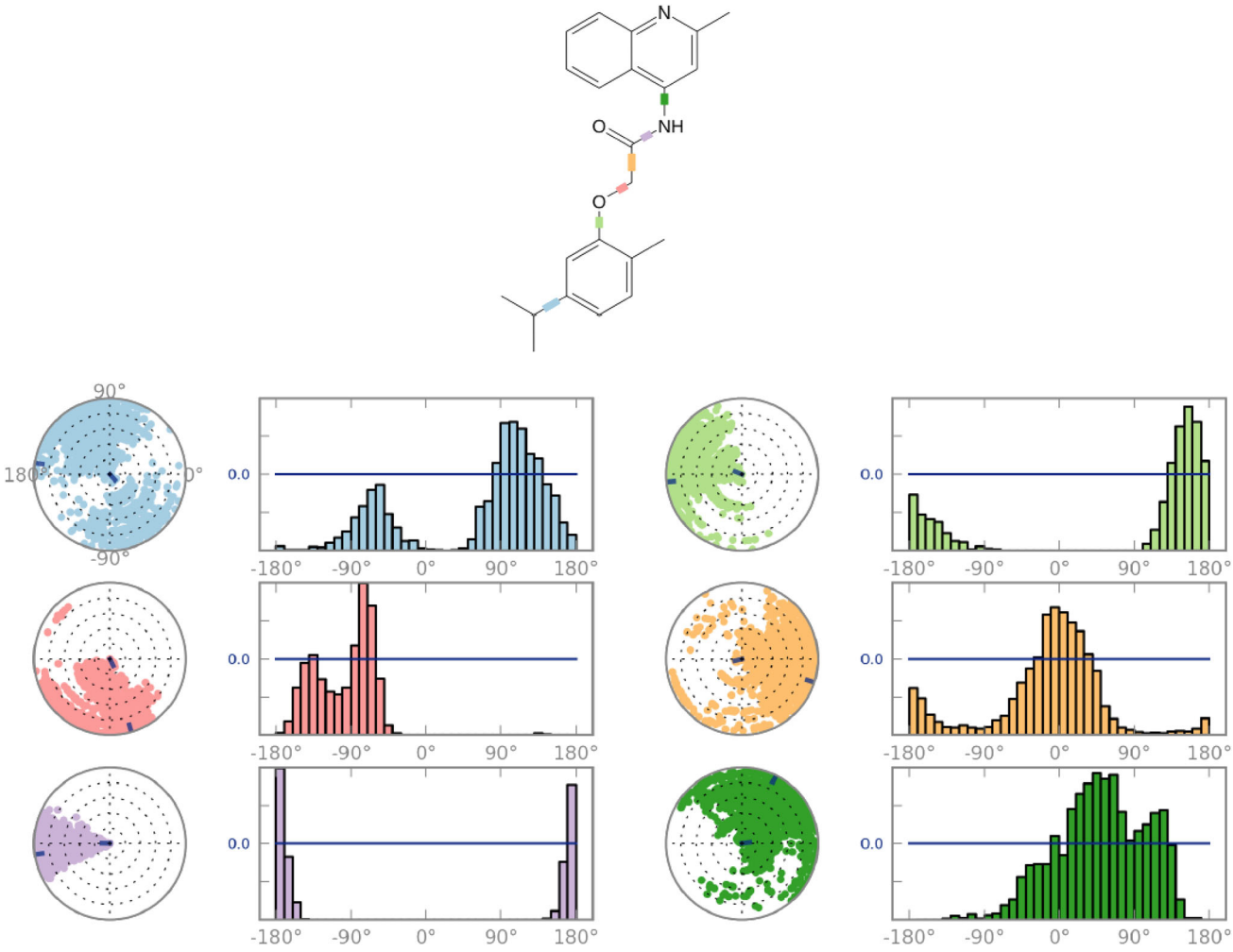

Figure 6. Torsional analysis of **5w** throughout MD simulations. (The ligand torsion plot summarizes the conformational evolution of every rotatable bond in the ligand throughout the simulation trajectory. The top panel shows the 2D schematic of a ligand with colour-coded rotatable bonds. Each rotatable bond torsion is accompanied by a dial plot and bar plots of the same colour.)

due to the strong polar and non-polar interactions forming between the ligands and the active site amino acids. The result of parallel artificial membrane permeability assay indicated that **5v** ($P_e = 4.38 \times 10^{-6}$ cm s^{-1}) showed greater permeability values than that limit, pointing out that these molecules would cross the BBB by passive diffusion.

Both docking and MD simulations were also repeated for known AChE and BuChE inhibitors, and results showed similar crucial amino acids interactions both in studied molecules and in known inhibitors.

Since BBB profiles are important for CNS drugs, we studied in detail the BBB properties of synthesized molecules; both MetaCore/MetaDrug and PAMPA-BBB results show that molecules can permeate the BBB. Thus, with this study, we improved the low inhibitory activity of carvacrol, and derivatives of carvacrol were able to penetrate through the BBB. Moreover, MetaCore/MetaDrug, which includes 26 different toxicity QSAR models, showed that studied molecules have less side effect predictions compared to known inhibitors.

Overall, these derivatives can be recommended as new chemotypes to develop new ChEs inhibitors for the treatment of AD disease.

4. Experimental section

4.1. General

All solvents, reagents and starting materials were obtained from commercial sources unless otherwise indicated. Melting points were taken on a Barnstead Electrothermal 9200. IR spectra were registered on a Bruker-Alpha infrared spectrometer. ^{1}H and ^{13}C NMR spectra were registered on a Varian Infinity Plus spectrometer at 300 and 75 Hz, respectively. 1 H and ^{13}C chemical shifts are referenced to the internal deuterated solvent. Mass spectra were obtained using Agilent GC-7890a and Agilent MS-5975c spectrometers. The elemental analyses were carried out with a Leco CHNS-932 instrument. Spectrophotometric analyses were performed by a BioTek Power Wave XS (BioTek, Winooski, VT). The electric eel AChE (Type-VI-S, EC 3.1.1.7, 425.84 U/mg, Sigma-Aldrich, St. Louis, MO) and horse serum butyrylcholinesterase (BuChE, EC 3.1.1.8, 11.4 U/mg, Sigma-Aldrich, St. Louis, MO) were purchased from Sigma-Aldrich (Steinheim, Germany). The other chemicals and solvents were purchased from Fluka Chemie, Merck (Kenilworth, NJ), Alfa Aaser (Ward Hill, MA) and Sigma-Aldrich (St. Louis, MO).

Table 3. Pharmacokinetic predictions of **5v** and **5w** using MetaCore/MetaDrug comprehensive systems biology analysis suite. ADME QSAR and protein binding QSAR models.

	5v	5w	Rivastigmine	Tacrine	Donepezil
BBB, log ratio[1]	0.24	0.25	0.22	0.40	0.05
G-Log*P*[2]	3.42	3.92	1.81	2.81	4.10
Prot-bind, %[3]	76.97	78.50	45.45	67.04	79.13
Prot-bind, Log *t*[4]	−0.02	−0.08	−0.12	0.04	0.24
WSol, log mg/L[5]	0.99	0.46	2.83	1.82	1.03
hERG-inh, pK_i[6]	0.29	0.21	−0.42	−0.82	0.42

Results are compared with positive control molecules rivastigmine, tacrine and donepezil.

[1]BBB penetration model. The data are expressed as log values of the ratio of the metabolite concentrations in brain and plasma. Cutoff is −0.3. Larger values indicate that the metabolite is more likely to enter the brain. Model description: $N = 107$, $R^2 = 0.89$, RMSE = 0.26.

[2]Lipophilicity, log of compound octanol–water distribution. Cutoffs are −0.4–5.6. Values greater than 5.6 correspond to overly hydrophobic compounds. Model description: $N = 13474$, $R^2 = 0.95$, RMSE = 0.21.

[3]Human serum protein binding, %. Cutoff is 50%. A value of more than 95% is highly bound, less than 50% is a low binding metabolite. Model description: $N = 265$, $R^2 = 0.909$, RMSE = 10.11.

[4]Affinity to human serum albumin, log value of the retention time. Cutoff is 0. Positive values correspond to higher protein binding and negative values to lower protein binding. The model is based on retention times of compounds assayed by HPLC using an immobilized HSA column. Values are expressed as log values of the retention time. Model description: $N = 95$, $R^2 = 0.904$, RMSE = 0.2.

[5]Water solubility at 25 °C, log mg/L. Cutoffs are from 2 to 4. An acceptable level of solubility is project dependent. Model description: $N = 2871$, $R^2 = 0.91$, RMSE = 0.54.

[6]Human hERG (human ether a-go-go-related gene) channel inhibition, p*Ki* (μM). Cutoff is −1.7. The higher the value, the higher the inhibition activity. Lower values are preferable. Model description: $N = 196$, $R^2 = 0.93$, RMSE = 0.23.

4.2. Synthesis of ethyl 2-(5-isopropyl-2-methylphenoxy) acetate (2)

Potassium carbonate (5.8 mmol) was added to a solution of carvacrol (5.7 mmol) and ethyl bromoacetate (5.7 mmol) in acetone (25 mL), and the reaction mixture was refluxed for 5 h. The mixture was filtrated and the solution was concentrated under reduced pressure, dried in vacuo and the solid obtained was crystallized from ethanol (Chimichi, Boccalini & Cosimelli, 2002). ^{1}H NMR ($CDCl_3$, 300 MHz) δ/ppm: 1.21 (6 H, d, $J = 6.7$ Hz), 1.29 (3 H, t, $J = 7.3$ Hz), 2.25 (3 H, s), 2.79-2.86 (1H,m), 4.23-4.30 (2 H, q), 4.63 (2 H, s), 6.57 (1 H, s), 6.77 (1 H, d, $J = 7.6$ Hz), 7.0 (1 H, d, $J = 7.6$ Hz); ^{13}C NMR ($CDCl_3$, 75 MHz) δ/ppm: 14.4, 15.5, 16.0, 24.2, 33.9, 34.2, 61.4, 66.1, 110.0, 113.2, 118.8, 119.5, 124.8, 131.0, 148.0, 153.9, 156.3, 169.5.

4.3. Synthesis of 2-(5-isopropyl-2-methylphenoxy)acetic acid (3)

The crude product **2** was dissolved in aqueous 10% NaOH (25 ml) and the solution was refluxed for 4 h. The reaction mixture was cooled and acidified with aqueous 6% HCl. The precipitated white solid was filtered off and subsequently washed with water to give compound **3** (Alipour et al., 2014). ^{1}H NMR ($CDCl_3$, 300 MHz) δ/ppm: 1.13 (6 H, d, $J = 7.0$ Hz), 2.11 (3 H, s), 2.73-2.80 (1H,m), 3.34 (1 H, s, OH), 4.65 (2 H, s), 6.65 (1 H, s), 6.7 (1 H, d, $J = 7.6$ Hz), 7.0 (1 H, d, $J = 7.4$ Hz); ^{13}C NMR ($CDCl_3$, 75 MHz) δ/ppm:

4.4. Synthesis of 2-(5-isopropyl-2-methylphenoxy)acetyl chloride (4)

3 mmol of $SOCl_2$ was added over 1 mmol of 2-(5-isopropyl-2-methylphenoxy)acetic acid (**3**) and stirred at room temperature for half an hour. It was then continued for 2 h at 80 °C. When the gas outlet was completed, the reaction was terminated and cooled. It was crystallized at ether and dried in vacuum. ^{1}H NMR ($CDCl_3$, 300 MHz) δ/ppm: 1.15 (6 H, d, $J = 7.0$ Hz), 2.13 (3 H, s), 2.75–2.84 (1H,m), 4.67 (2 H, s), 6.67 (1 H, s), 6.71 (1 H, d, $J = 7.6$ Hz), 7.0 (1 H, d, $J = 7.6$ Hz); ^{13}C NMR ($CDCl_3$, 75 MHz) δ/ppm: 16.3, 24.5, 34.0, 39.3, 41.0, 65.3, 110.2, 118.9, 123.8, 130.9, 147.9, 156.4, 171.1.

4.5. Synthesis of 2-(5-isopropyl-2-methylphenoxy)-N-R-acetamide (5a-w)

Compound **4** (1.0 mmol) and Et_3N (1.1 mmol) were dispersed in dry acetonitrile (5 ml). And then, appropriate amine (1.0 mmol) was added to the mixture. The mixture was stirred at 60 °C for overnight. The solvent was evaporated and the residue was washed with water. The resulting crude product was purified by column chromatography (Hexane:Ethylacetate).

2-(5-Isopropyl-2-methylphenoxy)-*N*-methylacetamide (**5a**): Brown liquid, 68% yield; IR: 3446, 3324, 2958, 2927, 2870, 1661, 1539, 1511, 1444, 1414, 1248, 1177, 1129, 995, 939, 850 cm^{-1}; ^{1}H NMR ($CDCl_3$, 300 MHz) δ/ppm: 1.12 (6 H, d, $J = 6.7$ Hz), 2.14 (3 H, s), 2.70–2.77 (1 H, m), 2.81 (3 H, d, $J = 4.9$ Hz), 4.39 (2 H, s), 6.53 (1 H, s), 6.64 (1 H, s, NH), 6.70 (1 H, d, $J = 7.6$ Hz), 6.97 (1 H, d, $J = 7.6$ Hz); ^{13}C NMR ($CDCl_3$, 75 MHz) δ/ppm: 16.2, 24.3, 26.0, 34.2, 67.7, 110.1, 119.7, 123.9, 131.1, 148.6, 155.6, 169.5. GC-MS (*m/z*): 221,1 [M^+]. Anal. Calcd. for $C_{13}H_{19}NO_2$: C, 70.56; H, 8.65; N, 6.33; found: C, 70.54; H, 8.61; N, 6.35.

2-(5-Isopropyl-2-methylphenoxy)-*N*-propylacetamide (**5b**): Yellow liquid, 58% yield; IR: 3428, 3305, 2960, 2930, 2873, 1659, 1614, 1580, 1538, 1512, 1442, 1250, 1177, 1130, 1057, 936, 815, 640, 563 cm^{-1}; ^{1}H NMR ($CDCl_3$, 300 MHz) δ/ppm: 0.93 (3 H, t, $J = 7.3$ Hz), 1.21 (6 H, d, $J = 7.0$ Hz), 1.54–1.61 (2 H, q), 2.24 (3 H, s), 2.83–2.87 (1 H, m), 3.35 (2 H, t, $J = 6.7$ Hz), 4.52 (2 H, s), 6.65 (1 H, s), 6.70 (1 H, s, NH), 6.81 (1 H, d, $J = 7.6$ Hz), 7.08 (1 H, d, $J = 7.6$ Hz); ^{13}C NMR ($CDCl_3$, 75 MHz) δ/ppm: 11.5, 16.1, 23.0, 24.2, 34.2, 40.9, 67.8, 110.2, 119.8, 123.9, 131.1, 148.7, 155.6, 168.8. GC-MS (*m/z*): 249,2 [M^+]. Anal. Calcd. for $C_{15}H_{23}NO_2$ C, 72.25; H, 9.30; N, 5.62; found: C, 72.28; H, 9.31; N, 5.63.

N,N-Diethyl-2-(5-isopropyl-2-methylphenoxy)acetamide (**5c**): Yellow liquid, 71% yield; IR: 2960, 2932, 2872, 1760, 1642, 1511, 1459, 1419, 1243, 1178, 1129, 1071, 1036, 813, 642, 463 cm^{-1}; ^{1}H NMR ($CDCl_3$, 300 MHz) δ/ppm: 1.12–1.24 (12 H, m), 2.23 (3 H, s), 2.83–2.88 (1 H, m), 3.38–3.48 (4 H, m), 4.69 (2 H, s), 6.73 (1 H, s), 6.76 (1 H, d, $J = 7.3$ Hz), 7.06 (1 H, d, $J = 7.6$ Hz); ^{13}C NMR ($CDCl_3$, 75 MHz) δ/ppm: 13.0, 14.6, 16.1, 24.3, 30.5, 34.2, 40.6, 41.9, 68.3, 109.9, 119.1, 124.2, 130.9, 148.2, 156.4, 167.8. GC-MS (*m/z*): 263,1 [M^+]. Anal. Calcd. for $C_{16}H_{25}NO_2$:C, 72.96; H, 9.57; N, 5.32; found: C, 72.92; H, 9.58; N, 5.33.

Table 4. Prediction of toxicity values using MetaCore/MetaDrug.

Property	5v	5w	Rivastigmine	Tacrine	Donepezil
AMES[1]	0.45	0.30	0.42	0.88	0.35
Anemia[2]	0.09	0.19	0.17	0.78	0.17
Carcinogenicity[3]	0.08	0.17	0.33	0.77	0.08
Carcinogenicity Mouse Female[4]	0.14	0.27	0.23	0.73	0.11
Carcinogenicity Mouse Male[5]	0.19	0.27	0.20	0.75	0.12
Carcinogenicity Rat Female[6]	0.04	0.21	0.22	0.83	0.02
Carcinogenicity Rat Male[7]	0.08	0.28	0.16	0.80	0.03
Cardiotoxicity[8]	0.29	0.26	0.78	0.63	0.75
Cytotoxicity Model, −log GI50 (M)[9]	5.33	5.15	5.29	5.11	5.21
Epididymis Toxicity[10]	0.16	0.51	0.14	0.53	0.04
Genotoxicity[11]	0.37	0.31	0.62	0.71	0.58
Hepatotoxicity[12]	0.17	0.34	0.27	0.75	0.14
Kidney Necrosis[13]	0.14	0.22	0.14	0.85	0.06
Kidney Weight Gain[14]	0.03	0.07	0.19	0.23	0.09
Liver Cholestasis[15]	0.27	0.39	0.56	0.61	0.62
Liver Lipid Accumulation[16]	0.13	0.22	0.38	0.55	0.29
Liver Necrosis[17]	0.22	0.14	0.31	0.82	0.78
Liver Weight Gain[18]	0.03	0.08	0.35	0.87	0.54
MRTD[19]	−0.02	0.21	0.37	0.34	0.22
Nasal Pathology[20]	0.09	0.11	0.22	0.26	0.04
Nephron Injury[21]	0.05	0.16	0.33	0.87	0.38
Nephrotoxicity[22]	0.08	0.24	0.08	0.36	0.12
Neurotoxicity[23]	0.21	0.41	0.38	0.63	0.18
Pulmonary Toxicity[24]	0.08	0.10	0.46	0.15	0.37
SkinSens, EC3[25]	50.30	24.73	32.04	5.66	21.85
Testicular Toxicity[26]	0.11	0.23	0.03	0.24	0.04

Results are compared with positive control molecules rivastigmine, tacrine and donepezil.

[1]Potential to be mutagenic (AMES positive), range from 0 to 1. A value of 1 is AMES positive (mutagenic) and a value of 0 is AMES negative (non-mutagenic). Cutoff is 0.5. Values close to zero are preferable. The AMES assay is based upon the reversion of mutations in the histidine operon in the bacterium *Salmonella enterica* sv Typhimurium.

[2]Potential for causing anaemia. Cutoff is 0.5. Values higher than 0.5 indicate potentially toxic compounds. Training set consists of chemicals and drugs causing anaemia *in vivo*. Model organisms: human. Model description: Training set $N = 324$, Test set $N = 51$, Sensitivity= 0.82, Specificity = 0.90, Accuracy = 0.86, MCC = 0.72.

[3]Potential for inducing carcinogenicity in rats and mice. Cutoff is 0.5. Values higher than 0.5 indicate potentially toxic compounds. Training set consists of chemicals and drugs causing carcinogenicity in vivo. Model organisms: mouse, rat. Model description: Training set $N = 1210$, Test set $N = 185$, Sensitivity= 0.96, Specificity = 0.90, Accuracy = 0.93, MCC = 0.86.

[4]Potential for inducing carcinogenicity in female mice. Cutoff is 0.5. Values higher than 0.5 indicate potentially toxic compounds. Training set consists of chemicals and drugs causing carcinogenicity *in vivo*. Model organisms: female mice. Model description: Training set $N = 640$, Test set $N = 94$, Sensitivity= 0.90, Specificity = 0.93, Accuracy = 0.92, MCC = 0.83.

[5]Potential for inducing carcinogenicity in male mice. Cutoff is 0.5. Values higher than 0.5 indicate potentially toxic compounds. Training set consists of chemicals and drugs causing carcinogenicity *in vivo*. Model organisms: mouse male. Model description: Training set $N = 584$, Test set $N = 93$, Sensitivity= 0.91, Specificity = 0.88, Accuracy = 0.89, MCC = 0.78.

[6]Potential for inducing carcinogenicity in female rats. Cutoff is 0.5. Values higher than 0.5 indicate potentially toxic compounds. Training set consists of chemicals and drugs causing carcinogenicity *in vivo*. Model organisms: female rat. Model description: Training set $N = 667$, Test set $N = 120$, Sensitivity= 0.90, Specificity = 0.96, Accuracy = 0.93, MCC = 0.86.

[7]Potential for inducing carcinogenicity in male rats. Cutoff is 0.5. Values higher than 0.5 indicate potentially toxic compounds. Training set consists of chemicals and drugs causing carcinogenicity *in vivo*. Model organisms: male rat. Model description: Training set $N = 715$, Test set $N = 117$, Sensitivity= 0.92, Specificity = 0.88, Accuracy = 0.90, MCC = 0.79.

[8]Potential for inducing cardiotoxicity. Cutoff is 0.5. Values higher than 0.5 indicate potentially toxic compounds. Training set consists of chemicals and drugs causing cardiotoxicity *in vivo*. Model organisms: mouse, rat, human. Model description: Training set $N = 143$, Test set $N = 30$, Sensitivity= 0.80, Specificity = 1.00, Accuracy = 0.90, MCC = 0.82.

[9]Growth inhibition of MCF7 cell line (human Caucasian breast adenocarcinoma), pGI50. Cutoff is 6. Values from 6 to 8 correspond to a toxic metabolite, values less than 6 are preferable, values less than 3 are more preferable and less toxic. Model description: $N = 1474$, $R^2 = 0.9$, RMSE = 0.05.

[10]Potential for inducing epididymis toxicity. Training set consists of chemicals and drugs causing epididymis toxicity *in vivo*. Model organisms: mouse, rat, human. Cutoff is 0.5. Values higher than 0.5 indicate potentially toxic compounds. Model description: Training set $N = 252$, Test set $N = 42$, Sensitivity= 0.90, Specificity = 0.86, Accuracy = 0.88, MCC = 0.76.

[11]Potential for inducing genotoxicity. Cutoff is 0.5. Values higher than 0.5 indicate potentially toxic compounds. Training set consists of chemicals and drugs causing genotoxicity *in vivo*. Model organisms: mouse, rat. Model description: Training set $N = 372$, Test set $N = 86$, Sensitivity= 0.75, Specificity = 0.84, Accuracy = 0.79, MCC = 0.59.

[12]Potential for inducing hepatotoxicity. Cutoff is 0.5. Values higher than 0.5 indicate potentially toxic compounds. Training set consists of chemicals and drugs causing hepatotoxicity *in vivo*. Model organisms: mouse, rat, human. Model description: Training set $N = 1380$, Test set $N = 231$, Sensitivity= 0.73, Specificity = 0.88, Accuracy = 0.81, MCC = 0.62.

[13]Potential for inducing kidney necrosis. Cutoff is 0.5. Values higher than 0.5 indicate potentially toxic compounds. Training set consists of chemicals and drugs causing renal necrosis *in vivo*. Model organisms: mouse, rat, human. Model description: Training set $N = 221$, Test set $N = 42$, Sensitivity= 0.96, Specificity = 1.00, Accuracy = 0.98, MCC = 0.95.

[14]Potential for inducing kidney weight gain. Cutoff is 0.5. The values higher than 0.5 indicate potentially toxic compounds. Training set consists of chemicals and drugs causing kidney weight gain *in vivo*. Model organisms: mouse, rat. Model description: Training set $N = 240$, Test set $N = 49$, Sensitivity= 0.95, Specificity = 1.00, Accuracy = 0.98, MCC = 0.96.

[15]Potential for inducing liver cholestasis. Cutoff is 0.5. Values higher than 0.5 indicate potentially toxic compounds. Training set consists of chemicals and drugs causing cholestasis *in vivo*. Model organisms: mouse, rat, human. Model description: Training set $N = 218$, Test set $N = 35$, Sensitivity= 0.79, Specificity = 0.67, Accuracy = 0.74, MCC = 0.46.

[16]Potential for inducing liver lipid accumulation. Cutoff is 0.5. Values higher than 0.5 indicate potentially toxic compounds. Training set consists of chemicals and drugs causing lipid accumulation *in vivo*. Model organisms: mouse, rat, human. Model description: Training set $N = 172$, Test set $N = 28$, Sensitivity= 0.80, Specificity = 0.85, Accuracy = 0.82, MCC = 0.64.

[17]Potential for inducing liver necrosis. Cutoff is 0.5. Values higher than 0.5 indicate potentially toxic compounds. Training set consists of chemicals and drugs causing hepatic necrosis *in vivo*. Model organisms: mouse, rat, human. Model description: Training set $N = 300$, Test set $N = 57$, Sensitivity= 0.91, Specificity = 0.91, Accuracy = 0.91, MCC = 0.82.

[18]Potential for inducing liver weight gain. Cutoff is 0.5. Values higher than 0.5 indicate potential liver weight-changing compounds. Training set consists of chemicals and drugs causing liver weight gain *in vivo*. Model organisms: mouse, rat. Model description: Training set $N = 292$, Test set $N = 52$, Sensitivity= 1.00, Specificity = 1.00, Accuracy = 1.00, MCC = 1.00.

[19]Maximum recommended therapeutic dose, log mg/kg-bm/day, range is from −5 to 3. Cutoff is 0.5. Chemicals with high log MRTDs can be classified as mildly toxic compounds, chemicals with low log MRTDs as highly toxic compounds. Model description: $N = 1209$, $R^2 = 0.86$, RMSE = 0.42.

[20]Potential for causing nasal pathology. Training set consists of chemicals and drugs causing nasal pathology *in vivo*. Model organisms: mouse, rat, human. Cutoff is 0.5. Values higher than 0.5 indicate potentially toxic compounds. Model description: Training set $N = 246$, Test set $N = 47$, Sensitivity= 1.00, Specificity = 0.93, Accuracy = 0.96, MCC = 0.92.

[21]Potential for inducing nephron injury. Cutoff is 0.5. Values higher than 0.5 indicate potentially toxic compounds. Training set consists of chemicals and drugs causing nephron injury *in vivo*. Model organisms: mouse, rat, human. Model description: Training set $N = 598$, Test set $N = 109$, Sensitivity= 0.91, Specificity = 1.00, Accuracy = 0.96, MCC = 0.93.

[22]Potential for inducing nephrotoxicity. Cutoff is 0.5. Values higher than 0.5 indicate potentially toxic compounds. Training set consists of chemicals and drugs causing nephrotoxicity *in vivo*. Model organisms: mouse, rat, human. Model description: Training set $N = 847$, Test set $N = 154$, Sensitivity= 0.90, Specificity = 0.84, Accuracy = 0.87, MCC = 0.74.

[23]Potential for inducing neurotoxicity. Training set consists of chemicals and drugs causing neurotoxicity *in vivo*. Model organisms: mouse, rat, human. Cutoff is 0.5. Values higher than 0.5 indicate potentially toxic compounds. Model description: Training set $N = 175$, Test set $N = 34$, Sensitivity= 0.94, Specificity = 0.94, Accuracy = 0.94, MCC = 0.88.

[24]Potential for inducing pulmonary toxicity. Training set consists of chemicals and drugs causing pulmonary toxicity *in vivo*. Model organisms: mouse, rat, human. Cutoff is 0.5. Values higher than 0.5 indicate potentially toxic compounds. Model description: Training set $N = 482$, Test set $N = 87$, Sensitivity= 0.89, Specificity = 0.88, Accuracy = 0.89, MCC = 0.77.

[25]Skin sensitization potential expressed as effective concentration 3, EC3%. Values higher than 10 indicate weak and moderate sensitizers. Model description: $N = 89$, $R^2 = 0.67$, RMSE = 22.56.

[26]It consists of chemicals and drugs causing testicular toxicity *in vivo*. Model organisms: mouse, rat, human. Cutoff is 0.5. Values higher than 0.5 indicate potentially toxic compounds. Model description: Training set $N = 439$, Test set $N = 88$, Sensitivity= 0.81, Specificity = 0.85, Accuracy = 0.83, MCC = 0.66.

Table 5. Prediction of blood–brain barrier penetration of drugs expressed as $P_e \pm$ SEM ($n = 4$–6).

	BBB penetration estimation	
Compound	P_e (10^{-6} cm s^{-1})	CNS (+/−)
5v	4.38 ± 0.54	CNS (+)
Tacrine	4.51 ± 0.32	CNS (+)
Donepezil	6.80 ± 0.66	CNS (+)
Rivastigmine	5.78 ± 0.85	CNS (+)

'CNS(+)' (High BBB permeation predicted; P_e (10^{-6} cm s^{-1}) >4.0.
'CNS(−)' (Low BBB permeation predicted; P_e (10^{-6} cm s^{-1}) <2.0.
'CNS(+/−)' (BBB permeation uncertain; P_e (10^{-6} cm s^{-1}) from 4.0 to 2.0.

N,N-Diisopropyl-2-(5-isopropyl-2-methylphenoxy)acetamide (**5d**): Yellow solid, 58% yield; mp.56 °C; IR: 2961, 2928, 2871, 1737, 1612, 1586, 1443, 1422, 1342, 1239, 1175, 1127, 1034, 871, 812, 735, 590 cm^{-1}; ^{1}H NMR ($CDCl_3$, 300 MHz) δ/ppm: 1.10–1.15 (12 H, m), 1.34 (6 H, d, $J = 7.0$ Hz), 2.13 (3 H, s), 2.72–2.79 (1 H, m), 3.31–3.35 (1 H, m), 4.12–4.16 (1 H, m), 4.55 (2 H, s), 6,66 (1 H, d, $J = 7.9$ Hz), 6,67 (1H,s), 6.96 (1 H, d, $J = 7.9$ Hz); ^{13}C NMR ($CDCl_3$, 75 MHz) δ/ppm: 16.2, 20.5, 21.1, 24.3, 30.5, 34.3, 46.3, 49.0, 69.7, 109.5, 118.9, 123.9, 130.8, 148.3, 156.3, 167.6. GC-MS (*m/z*): 291,1 [M^+]. Anal. Calcd. for $C_{18}H_{29}NO_2$: C, 74.18; H, 10.03; N, 4.81; found: C, 74.20; H, 10.07; N, 4.80.

N-Cyclohexyl-2-(5-isopropyl-2-methylphenoxy)acetamide (**5e**): Light yellow solid, 62% yield; mp. 78.3 °C; IR: 3292, 2956, 2929, 2852, 1665, 1613, 1578, 1536, 1417, 1277, 1244, 1140, 971, 847, 715, 644, 585 cm^{-1}; ^{1}H NMR ($CDCl_3$, 300 MHz) δ/ppm: 1.20-1.29 (10 H, m), 1.32–1.47 (2H,m), 1.59–1.73 (2H,m), 1.90–1.96 (2 H, m), 2.24 (3 H, s), 2.81–2.90 (1H,m), 3.85–3.88 (1 H, m), 4.49 (2 H, s), 6.52–6.53 (1 H, s, NH), 6.65 (1 H, s), 6.80 (1 H, d, $J = 7.6$ Hz), 7.09 (1 H, d, $J = 7.6$ Hz); ^{13}C NMR ($CDCl_3$, 75 MHz) δ/ppm: 16.1, 24.2, 24.8, 25.6, 33.1, 34.2, 47.8, 67.8, 110.3, 119.8, 123.8, 131.0, 148.7, 155.6, 168.0. GC-MS (*m/z*): 289,2 [M^+]. Anal. Calcd. for $C_{18}H_{27}NO_2$: C, 74.70; H, 9.40; N, 4.84; found: C, 74.73; H, 9.42; N, 4.82.

2-(5-Isopropyl-2-methylphenoxy)-1-(pyrrolidin-1-yl)ethanone (**5f**): White liquid, 40% yield; IR: 2957, 2927, 2872, 1641, 1580, 1511, 1448, 1418, 1340, 1288, 1247, 1177, 1131, 1038, 993, 858, 813, 716, 642, 522, 463 cm^{-1}; ^{1}H NMR ($CDCl_3$, 300 MHz) δ/ppm: 1.21 (6 H, d, $J = 7.0$ Hz), 1.81–1.95 (4 H, m), 2.22 (3 H, s), 2.80–2.87 (1 H, m), 3.51 (2 H, t, $J = 6.7$ Hz), 3.55 (2 H, t, $J = 6.7$ Hz), 4.62 (2 H, s), 6,72 (1 H, s), 6,76 (1 H, d, $J = 7.9$ Hz), 7.05 (1 H, d, $J = 7.9$ Hz); ^{13}C NMR ($CDCl_3$, 75 MHz) δ/ppm: 16.1, 24.0, 24.3, 26.5, 34.2, 46.4, 68.8, 109.9, 119.1, 124.2, 130.9, 148.3, 156.3, 167.2. GC-MS (*m/z*): 261,1 [M^+]. Anal. Calcd. for $C_{16}H_{23}NO_2$: C, 73.53; H, 8.87; N, 5.36; found: C, 73.52; H, 8.85; N, 5.38.

2-(5-Isopropyl-2-methylphenoxy)-1-(piperidin-1-yl)ethanone (**5g**): Light brown liquid, 45% yield; IR: 2970, 2860, 1771, 1642, 1613, 1511, 1445, 1418, 1240, 1176, 1120, 1039, 997, 852, 813, 642, 575 cm^{-1}; ^{1}H NMR ($CDCl_3$, 300 MHz) δ/ppm: 1.23 (6 H, d, $J = 6.7$ Hz), 1.55–1.64 (6 H, m), 2.21 (3 H, s), 2.83–2.88 (1 H, m), 3.52–3.59 (4 H, m), 4.68 (2 H, s), 6.73 (1 H, s), 6.77 (1 H, d, $J = 7.9$ Hz), 7.04 (1 H, d, $J = 7.3$ Hz); ^{13}C NMR ($CDCl_3$, 75 MHz) δ/ppm: 16.1, 24.3, 24.7, 25.7, 26.7, 34.3, 43.5, 46.8, 68.4, 109.7, 119.0, 124.1, 130.8, 148.3, 156.1, 166.8. GC-MS (*m/z*): 275,1 [M^+]. Anal. Calcd. for $C_{17}H_{25}NO_2$: C, 74.14; H, 9.15; N, 5.09; found: C, 74.16; H, 9.17; N, 5.06.

2-(5-Isopropyl-2-methylphenoxy)-1-morpholinoethanone (**5h**): White solid, 40% yield; mp. 79 °C; IR 2979, 2958, 2907, 2879, 1653, 1610, 1577, 1502, 1461, 1433, 1302, 1234, 1176, 1113, 1031, 851, 818, 760, 566 cm^{-1}; ^{1}H NMR ($CDCl_3$, 300 MHz) δ/ppm: 1.22 (6 H, d, $J = 7.0$ Hz), 2.18 (3 H, s), 2.81–2.88 (1 H, m), 3.64 (8 H, s), 4.68 (2 H, s), 6.72 (1 H, s), 6.77 (1 H, d, $J = 7.6$ Hz), 7.06 (1 H, d, $J = 7.6$ Hz); ^{13}C NMR ($CDCl_3$, 75 MHz) δ/ppm: 16.0, 24.3, 34.3, 42.7, 46.3, 67.0, 68.2, 109.6, 119.3, 123.9, 131.0, 148.5, 155.8, 167.1. GC-MS (*m/z*): 277,1 [M^+]. Anal. Calcd. for $C_{16}H_{23}NO_2$: C, 69.29; H, 8.36; N, 5.05; found: C, 69.27; H, 8.34; N, 5.07.

N-(2,3-Dihydro-1*H*-inden-2-yl)-2-(5-isopropyl-2-methylphenoxy)acetamide (**5i**): Yellow liquid, 50% yield; IR: 3327, 3068, 3026, 2960, 2930, 2866, 1655, 1540, 1485, 1248, 1128, 1059, 1019, 947, 860, 800, 734, 639, 585, 565, 459 cm^{-1}; ^{1}H NMR ($CDCl_3$, 300 MHz) δ/ppm: 1.21 (6 H, d, $J = 7.0$ Hz), 2.09 (3 H, s), 2.80–2.87 (1H,m), 2.84 (2 H, dd, $J = 5.2$; 15.8 Hz), 3.37 (2 H, dd, $J = 7.3$; 16.1 Hz), 4.49 (2 H, s), 4.81–4.87 (1 H, m), 6.63 (1 H, s), 6.79 (1 H, d, $J = 7.6$ Hz), 6.80 (1 H, s, NH), 7.04 (1 H, d, $J = 7.6$ Hz), 7.16–7.26 (4 H, m); ^{13}C NMR ($CDCl_3$, 75 MHz) δ/ppm: 15.9, 24.2, 34.2, 40.2, 50.3, 67.9, 110.4, 119.9, 123.9, 124.9, 127.1, 131.0, 131.1, 140.7, 148.7, 155.5, 168.5. GC-MS (*m/z*): 323,1 [M^+]. Anal. Calcd. for $C_{21}H_{25}NO_2$: C, 77.98; H, 7.79; N, 4.33; found: C, 77.96; H, 7.76; N, 4.35.

2-(5-Isopropyl-2-methylphenoxy)-*N*-(2-(pyrrolidin-1-yl)ethyl) acetamide (**5j**): Brown liquid, 62% yield; IR: 3390, 2958, 2929, 2874, 2797, 1677, 1614, 1582, 1511, 1418, 1344, 1250, 1178, 1130, 1055, 994, 877, 814, 640, 573, 422 cm^{-1}; ^{1}H NMR ($CDCl_3$, 300 MHz) δ/ppm: 1.21 (6 H, d, $J = 6.7$ Hz), 1.71–1.76 (4 H, m), 2.23 (3 H, s), 2.44–2.50 (4 H, m), 2.63 (2 H, t, $J = 6.1$ Hz), 2.80–2.86 (1H,m), 3.40–3.46 (2 H, m), 4.49 (2 H, s), 6.63 (1 H, s), 6.78 (1 H, d, $J = 7.6$ Hz), 7.07 (1 H, d, $J = 7.6$ Hz), 7.43 (1 H, s, NH); ^{13}C NMR ($CDCl_3$, 75 MHz) δ/ppm: 15.9, 23.7, 24.3, 34.2, 37.5, 53.8, 54.1, 67.3, 109.7, 119.5, 123.9, 131.0, 148.5, 155.5, 168.6. GC-MS (*m/z*): 304,2 [M^+]. Anal. Calcd. for $C_{18}H_{28}N_2O_2$: C, 71.02; H, 9.27; N, 9.20; found: C, 71.04; H, 9.25; N, 9.23.

2-(5-Isopropyl-2-methylphenoxy)-*N*-(2-morpholinoethyl)acetamide (**5k**): Yellow liquid, 66% yield; IR: 3404, 2958, 2856, 2813, 1677, 1511, 1445, 1418, 1297, 1251, 1178, 1116, 1055, 1036, 867, 815, 763, 640, 575, 446 cm^{-1}; ^{1}H NMR ($CDCl_3$, 300 MHz) δ/ppm: 1.13 (6 H, d, $J = 7.6$ Hz), 2.22 (3 H, s), 2.32–2.35 (4 H, m), 2.43 (2 H, t, $J = 6.1$ Hz), 2.73–2.82 (1H,m), 3.33–3.38 (2 H, m), 3.53–3.56 (4 H, m), 4.44 (2 H, s), 6.55 (1 H, s), 6.71 (1 H, d, $J = 7.6$ Hz), 7.01 (1 H, d, $J = 7.6$ Hz), 7.25 (1 H, s, NH); ^{13}C NMR ($CDCl_3$, 75 MHz) δ/ppm: 16.4, 24.3, 34.2, 35.1, 53.4, 56.8, 67.1, 67.1, 109.5, 119.5, 123.6, 131.0, 148.6, 155.4, 168.5. GC-MS (*m/z*): 320,2 [M^+]. Anal. Calcd. for $C_{18}H_{28}N_2O_3$: C, 67.47; H, 8.81; N, 8.74; found: C, 67.45; H, 8.83; N, 8.76.

N-(2-(Cyclohex-1-en-1-yl)ethyl)-2-(5-isopropyl-2-methylphenoxy)acetamide (**5l**): Brown liquid, 82% yield; IR: 3417, 3306, 2957, 2925, 2836, 1674, 1525, 1511, 1418, 1248, 1177, 1130, 1055, 814, 639, 555, 448 cm^{-1}; ^{1}H NMR ($CDCl_3$, 300 MHz) δ/ppm: 1.22 (6 H, d, $J = 6.7$ Hz), 1.49–1.63 (4 H, m), 1.91–2.09 (4 H, m), 2.17 (2 H, t, $J = 6.4$ Hz), 2.22 (3 H, s), 2.81-2.90 (1H,m), 3.40–3.46 (2 H, q), 4.49 (2 H, s), 5.43 (1 H, s), 6.63 (1 H, s), 6.66 (1 H, s, NH), 6.80 (1 H, d, $J = 7.6$ Hz), 7.1 (1 H, d, $J = 7.6$ Hz); ^{13}C NMR ($CDCl_3$, 75 MHz) δ/ppm: 16.1, 22.5, 22.9, 24.3, 25.4, 27.8,

34.3, 36.3, 37.5, 67.3, 109.7, 119.6, 123.7, 124.4, 131.0, 134.4, 148.6, 155.4, 168.5. GC-MS (*m/z*): 315,2 [M^+]. Anal. Calcd. for $C_{20}H_{29}NO_2$: C, 76.15; H, 9.27; N, 4.44; found: C, 76.18; H, 9.24; N, 4.46.

N-(3,4-Dimethoxyphenethyl)-2-(5-isopropyl-2-methylpheno xy)acetamide (**5m**): Light brown liquid, 60% yield; IR: 3416, 3359, 2957, 2932, 2869, 2835, 1673, 1612, 1512, 1441, 1417, 1381, 1257, 1177, 1130, 1027, 939, 852, 812, 638, 558 cm^{-1}; ^1H NMR ($CDCl_3$, 300 MHz) δ/ppm: 1.21 (6 H, d, $J = 6.7$ Hz), 2.06 (3 H, s), 2.80 (2 H, t, $J = 6.7$ Hz), 2.84-2.86 (1H,m), 3.60-3.66 (2 H, q), 3.83 (3 H, s), 3.85 (3 H, s), 4.48 (2 H, s), 6.61–6.81 (6 H, m), 7.0 (1 H, d, $J = 7.6$ Hz); ^{13}C NMR ($CDCl_3$, 75 MHz) δ/ppm: 16.0, 24.2, 34.2, 35.3, 40.1, 56.0, 56.1, 67.5, 110.0, 111.6, 111.9, 119.7, 120.8, 123.8, 131.0, 148.0, 148.6, 149.4, 155.4, 168.8. GC-MS (*m/z*): 371,2 [M^+]. Anal. Calcd. for $C_{22}H_{29}NO_4$: C, 71.13; H, 7.87; N, 3.77; found: C, 71.15; H, 7.85; N, 3.80.

N-(Benzo[*d*][1,3]dioxol-5-ylmethyl)-2-(5-isopropyl-2-methyl-phenoxy)acetamide (**5n**): Light yellow solid, 74% yield; mp.66.8 °C; IR 3307, 2963, 2930, 2876, 2784, 1649, 1534, 1486, 1429, 1375, 1239, 1175, 1126, 1007, 926, 824, 771, 716, 676, 578, 455, 419 cm^{-1}; ^1H NMR ($CDCl_3$, 300 MHz) δ/ppm: 1.21 (6 H, d, $J = 7.0$ Hz), 2.19 (3 H, s), 2.80-2.87 (1H,m), 4.45 (2 H, d, $J = 6.1$ Hz), 4.55 (2 H, s), 5.93 (2 H, s), 6.64 (1 H, s), 6.74–6.86 (5 H, m, NH), 7.07 (1 H, d, $J = 7.6$ Hz); ^{13}C NMR ($CDCl_3$, 75 MHz) δ/ppm: 16.1, 24.2, 34.2, 42.9, 67.9, 101.3, 108.4, 108.5, 110.3, 119.9, 121.0, 124.0, 131.1, 131.9, 147.2, 148.7, 155.6, 168.7. GC-MS (*m/z*): 342.9 [M^+]. Anal. Calcd. for $C_{20}H_{23}NO_4$: C, 70.36; H, 6.79; N, 4.10; found: C, 70.38; H, 6.77; N, 4.12.

2-(5-Isopropyl-2-methylphenoxy)-*N*-morpholinoacetamide (**5o**): Beige solid, 70% yield; mp.107 °C; IR: 3199, 3064, 2969, 2948, 2864, 2824, 1737, 1666, 1559, 1513, 1460, 1449, 1415, 1242, 1106, 1022, 974, 917, 864, 804, 714, 647, 586, 478 cm^{-1}; ^1H NMR ($CDCl_3$, 300 MHz) δ/ppm: 1.21 (6 H, d, $J = 6.5$ Hz), 2.25 (3 H, s), 2.81–2.89 (5H,m), 3.83–3.86 (4 H, m), 4.55 (2 H, s), 6.64 (1 H, s), 6.83 (1 H, d, $J = 8.4$ Hz), 7.1 (1 H, d, $J = 7.6$ Hz), 7.32 (1 H, s, NH); ^{13}C NMR ($CDCl_3$, 75 MHz) δ/ppm: 16.1, 24.2, 34.2, 56.2, 66.4, 67.7, 110.7, 120.1, 123.8, 131.2, 148.8, 155.4, 166.1. GC-MS (*m/z*): 292,1 [M^+]. Anal. Calcd. for $C_{16}H_{24}N_2O_3$: C, 65.73; H, 8.27; N, 9.58; found: C, 65.75; H, 8.29; N, 9.55.

2-(5-Isopropyl-2-methylphenoxy)-N-(4-methylpiperazin-1-yl) acetamide (**5p**): Light brown solid, 68% yield; mp.103 °C; IR: 3207, 3068, 2955, 2932, 2825, 2795, 2745, 1660, 1613, 1561, 1455, 1415, 1241, 1178, 1131, 1064, 1014, 971, 811, 706, 588, 461 cm^{-1}; ^1H NMR ($CDCl_3$, 300 MHz) δ/ppm: 1.21 (6 H, d, $J = 7.0$ Hz), 2.23 (3 H, s), 2.32 (3 H, s), 2.60–2.63 (4H,m), 2.83–2.88 (5 H, m), 4.54 (2 H, s), 4.65 (1 H, s, NH), 6.63 (1 H, s), 6.82 (1 H, d, $J = 7.6$ Hz), 7.1 (1 H, d, $J = 7.6$ Hz); ^{13}C NMR ($CDCl_3$, 75 MHz) δ/ppm: 16.1, 24.2, 34.2, 45.8, 54.2, 55.7, 67.7, 110.1, 120.1, 123.8, 131.1, 148.7, 155.4, 165.9. GC-MS (*m/z*): 305,2 [M^+]. Anal. Calcd. for $C_{17}H_{27}N_3O_2$: C, 66.85; H, 8.91; N, 13.76; found: C, 66.87; H, 8.90; N, 13.74.

2-(5-Isopropyl-2-methylphenoxy)-N-(piperidin-1-yl)acetamide (**5q**): Yellow solid, 74% yield; mp. 94 °C; IR: 3211, 3066, 2942, 2924, 2864, 2811, 1668, 1557, 1513, 1453, 1414, 1240, 1179, 1140, 1128, 1060, 990, 849, 805, 712, 579, 546, 453, 433 cm^{-1}; ^1H NMR ($CDCl_3$, 300 MHz) δ/ppm: 1.22 (6 H, d, $J = 7.0$ Hz), 1.44–1.48 (2 H, m), 1.72–1.77 (4 H, m), 2.25 (3 H, s), 2.80–2.87 (5 H, m), 4.54 (2 H, s), 6.64 (1 H, s), 6.82 (1 H, d, $J = 7.6$ Hz), 7.1 (1 H, d, $J = 7.6$ Hz), 7.27 (1 H, s, NH); ^{13}C NMR ($CDCl_3$, 75 MHz) δ/ppm: 16.2, 23.3, 24.2, 25.3, 34.2, 57.4, 67.7, 110.0, 120.0, 123.8, 131.1, 148.7, 155.5, 165.7. GC-MS (*m/z*): 290,2 [M^+]. Anal. Calcd. for $C_{17}H_{26}N_2O_2$: C, 70.31; H, 9.02; N, 9.65; found: C, 74.33; H, 9.05; N, 9.62.

N-(3-(Dimethylamino)propyl)-2-(5-isopropyl-2-methylpheno xy)acetamide (**5r**): Yellow liquid, 50% yield; IR: 3337, 2957, 2867, 2818, 2770, 1665, 1529, 1512, 1459, 1418, 1248, 1177, 1130, 1056, 994, 852, 814, 641, 581, 461 cm^{-1}; ^1H NMR ($CDCl_3$, 300 MHz) δ/ppm: 1.19 (6 H, d, $J = 6.7$ Hz), 1.60–1.68 (2 H, m), 2.06 (6 H, s), 2.22 (3 H, s), 2.28–2.32 (2 H, m), 2.80–2.84 (1H,m), 3.39-3.45 (2 H, m), 4.48 (2 H, s), 6.60 (1 H, s), 6.75 (1 H, d, $J = 7.6$ Hz), 7.04 (1 H, d, $J = 7.6$ Hz), 7.7 (1 H, s, NH, br); ^{13}C NMR ($CDCl_3$, 75 MHz) δ/ppm: 16.1, 24.3, 26.2, 34.2, 39.1, 45.5, 58.8, 67.7, 109.9, 119.5, 123.9, 130.9, 148.5, 155.8, 168.8. GC-MS (*m/z*): 292,1 [M^+]. Anal. Calcd. for $C_{17}H_{28}N_2O_2$: C, 69.83; H, 9.65; N, 9.58; found: C, 69.80; H, 9.63; N, 9.59.

1-(4-Benzylpiperidin-1-yl)-2-(5-isopropyl-2-methylphenoxy) ethanone (**5s**): White liquid, 86% yield; IR: 3060, 3024, 2911, 2853, 2771, 2729, 1646, 1512, 1452, 1417, 1367, 1232, 1136, 1056, 991, 826, 748, 697, 634, 591, 461 cm^{-1}; ^1H NMR ($CDCl_3$, 300 MHz) δ/ppm: 1.13–1.19 (2 H, m), 1.22 (6 H, d, $J = 7.0$ Hz), 1.67–1.78 (3 H, m), 2.20 (3 H, s), 2.50–2.57 (3 H, m), 2.81–2.88 (1 H, m), 2.93-3.03 (1 H, m), 4.05 (1 H, d, $J = 13.4$ Hz), 4.56 (1 H, d, $J = 11.4$ Hz), 4.66 (2 H, d, $J = 4.9$ Hz), 6.71 (1 H, s), 6.77 (1 H, d, $J = 7.6$ Hz), 7.05–7.12 (3 H, m), 7.17–7.30 (3 H, m); ^{13}C NMR ($CDCl_3$, 75 MHz) δ/ppm: 16.2, 24.4, 31.9, 32.9, 34.3, 38.4, 42.8, 43.2, 46.0, 68.4, 109.8, 119.1, 124.1, 126.3, 128.6, 129.3, 130.9, 140.1, 148.4, 156.2, 166.7. GC-MS (*m/z*): 365,2 [M^+]. Anal. Calcd. for $C_{24}H_{31}NO_2$: C, 78.86; H, 8.55; N, 3.83; found: C, 78.84; H, 8.57; N, 3.85.

2-(5-Isopropyl-2-methylphenoxy)-*N*-(pyridin-2-yl)acetamide (**5t**): Yellow liquid, 56% yield; IR: 3394, 2957, 2924, 2867, 1698, 1667, 1577, 1521, 1415, 1307, 1256, 1168, 1134, 1056, 775, 678, 571, 514 cm^{-1}; ^1H NMR ($CDCl_3$, 300 MHz) δ/ppm: 1.23 (6 H, d, $J = 7.0$ Hz), 2.35 (3 H, s), 2.85–2.89 (1 H, m), 4.65 (2 H, s), 6.70 (1 H, s), 6.83 (1 H, d, $J = 7.6$ Hz), 7.07–7.14 (2 H, m), 7.74 (1 H, t, $J = 8.4$ Hz), 8.26–8.34 (2 H, m), 8.96 (1 H, s, NH); ^{13}C NMR ($CDCl_3$, 75 MHz) δ/ppm: 16.3, 24.3, 34.2, 67.9, 110.4, 114.3, 120.1, 120.5, 124.3, 131.2, 138.6, 148.3, 148.6, 150.6, 155.3, 167.4. GC-MS (*m/z*): 284,1 [M^+]. Anal. Calcd. for $C_{17}H_{20}N_2O_2$: C, 71.81; H, 7.09; N, 9.85; found: C, 71.83; H, 7.11; N, 9.83.

2-(5-isopropyl-2-methylphenoxy)-N-(pyrimidin-2-yl)aceta-mide (**5u**): White solid, 60% yield; IR: 3144, 3072, 2958, 2919, 2866, 1705, 1582, 1512, 1451, 1403, 1278, 1255, 1227, 1181, 1133, 1074, 848, 811, 637, 536, 414 cm^{-1}; ^1H NMR ($CDCl_3$, 300 MHz) δ/ppm: 1.23 (6 H, d, $J = 7.1$ Hz), 2.35 (3 H, s), 2.82-2.89 (1H,m), 4.72 (2 H, s), 6.71 (1 H, s), 6.83 (1 H, d, $J = 7.7$ Hz), 7.09–7.15 (2 H, m), 8.7 (2 H, d, $J = 5.5$ Hz), 9.1 (1 H, s, NH); ^{13}C NMR ($CDCl_3$, 75 MHz) δ/ppm: 16.3, 24.3, 34.2, 68.1, 110.3, 117.5, 120.2, 124.1, 131.2, 148.7, 155.2, 157.0, 158.8, 166.8. GC-MS (*m/z*): 285,1 [M^+]. Anal. Calcd. for $C_{16}H_{19}N_3O_2$: C, 67.35; H, 6.71; N, 14.73; found: C, 67.37; H, 6.72; N, 14.70.

2-(5-Isopropyl-2-methylphenoxy)-*N*-(quinolin-8-yl)acetamide (**5v**): Purple solid, 40% yield; mp. 127.5 °C; IR: 3323, 3046,

2956, 2886, 2866, 1679, 1578, 1535, 1417, 1257, 1173, 1131, 1057, 996, 939, 827, 808, 750, 640, 572, 465, 422 cm^{-1}; ^1H NMR ($CDCl_3$, 300 MHz) δ/ppm: 1.25 (6 H, d, $J = 6.7$ Hz), 2.57 (3 H, s), 2.87–2.92 (1H,m), 4.74 (2 H, s), 6.77 (1 H, s), 6.84 (1 H, d, $J = 7.6$ Hz), 7.17 (1 H, d, $J = 7.6$ Hz), 7.44–7.49 (1 H, m), 7.55–7.57 (2 H, m), 8.17 (1 H, d, $J = 8.2$ Hz), 8.81–8.83(2H, m), 11.2 (1 H, s, NH); ^{13}C NMR ($CDCl_3$, 75 MHz) δ/ppm: 16.2, 24.3, 34.3, 67.7, 109.8, 116.8, 119.6, 121.9, 122.3, 124.4, 127.5, 128.1, 131.1, 134.0, 136.4, 139.0, 148.5, 148.6, 155.5, 167.0. GC-MS (*m/z*): 334,1 [M^+]. Anal. Calcd. for $C_{21}H_{22}N_2O_2$: C, 75.42; H, 6.63; N, 8.38; found: C, 75.46; H, 6.65; N, 8.40.

2-(5-Isopropyl-2-methylphenoxy)-N-(2-methylquinolin-4-yl) acetamide (**5w**): White solid, 56% yield; mp. 111 °C; IR: 3402, 2956, 2916, 2868, 1706, 1616, 1532, 1498, 1418, 1250, 1178, 1128, 1053, 999, 978, 949, 865, 801, 746, 646, 624, 579, 533, 462 cm^{-1}; ^1H NMR ($CDCl_3$, 300 MHz) δ/ppm: 1.25 (6 H, d, $J = 7.0$ Hz), 2.44 (3 H, s), 2.75 (3 H, s), 2.85–2.94 (1H,m), 4.75 (2 H, s), 6.76 (1 H, s), 6.90 (1 H, d, $J = 7.6$ Hz), 7.18 (1 H, d, $J = 7.6$ Hz), 7.32 (1 H, t, $J = 8.2$ Hz), 7.67–7.75 (2 H, q), 8.0 (1 H, d, $J = 8.5$ Hz), 8.3 (1 H, s), 9.3 (1 H, s, NH); ^{13}C NMR ($CDCl_3$, 75 MHz) δ/ppm: 16.6, 24.3, 26.0, 34.3, 67.8, 110.2, 111.5, 118.4, 118.5, 120.4, 123.6, 126.1, 129.8, 130.0, 131.4, 139.3, 148.6, 149.0, 154.9, 160.4, 167.3. GC-MS (*m/z*): 348,1 [M^+]. Anal. Calcd. for $C_{22}H_{24}N_2O_2$: C, 75.83; H, 6.94; N, 8.04; found: C, 75.85; H, 6.96; N, 8.07.

4.6. Anticholinesterase activity assays

AChE and BuChE inhibitory activities of the synthesized compounds were determined according to Ellman's method. The IC_{50} was determined by constructing an absorbance and/or inhibition (%) curve and examining the effect of five different concentrations. IC_{50} values were calculated for a given antagonist by determining the concentration needed to inhibit half of the maximum biological response of the agonist. The substrates of the reaction were acetylthiocholine iodide and butyrylthiocholine iodide. 5,5′-Dithio-bis(2-nitrobenzoic) acid (DTNB) was used to measure anticholinesterase activity. Stock solutions of the compounds and galantamine in methanol were prepared at a concentration of 4000 μg/mL. Aliquots of 150 μL of 100 mM phosphate buffer (pH 8.0), 10 μL of sample solution and 20 μL AChE (2.476×10^{-4} U/μL) (or 3.1813×10^{-4} U/μL BuChE) solution were mixed and incubated for 15 min at 25 °C. 10 μL of DTNB solution was prepared by adding 2.0 mL of pH 7.0 and 4.0 mL of pH 8.0 phosphate buffers to a mixture of 1.0 mL of 16 mg/mL DTNB and 7.5 mg/mL $NaHCO_3$ in pH 7.0 phosphate buffers. The reaction was initiated by the addition of 10 μL acetylthiocholine iodide (or butyrylthiocholine iodide). In this method, the activity was measured by following the yellow colour produced as a result of the thio anion produced by reacting the enzymatic hydrolysis of the substrate with DTNB. Also, methanol was used as a control solvent. The hydrolysis of the substrates was monitored using a BioTek Power Wave XS at 412 nm.

4.7. In vitro BBB permeation assay

The Corning Gentest Pre-coated PAMPA Plate System (Cat. No. 353015) was used to perform permeability assays for novel compounds (Chen, Murawski, Patel, Crespi, & Balimane, 2008). In summary, the 96-well filter plate, pre-coated with lipids, was used as the permeation acceptor and a matching 96-well receiver plate was used as the permeation donor. Compound solutions were prepared by diluting 10 mM DMSO stock solutions in PBS (in most cases, we used a final concentration of 200 μM). The compound solutions were added to the wells (300 μL/well) of the receiver plate and PBS was added to the wells (200 μL/well) of the pre-coated filter plate. The filter plate was then coupled with the receiver plate, and the plate assembly was incubated at room temperature without agitation for 5 h. At the end of the incubation, the plates were separated and 150 μL solution from each well of both the filter plate and the receiver plate was transferred to UV-transparent plates. The final concentrations of compounds in both donor wells and acceptor wells were analysed by a UV plate reader Synergy H1 (BioTek, USA). Concentration of the compound was calculated from the standard curve and expressed as permeability (P_e) following the formula:

Permeability (cm/s): $Pe = \{-\ln[1-CA(t)/Ceq]\}/[A^*(1/VD+1/VA)^*t]$

A = filter area (0.3 cm^2),

V_D = donor well volume (0.3 mL),

V_A = acceptor well volume (0.2 mL), t = incubation time,

$C_A(t)$ = compound concentration in acceptor well at time t,

$C_D(t)$ = compound concentration in donor well at time t,

$C_{eq} = [C_D(t) \times V_D + C_A(t) \times V_A]/(V_D + V_A)$.

4.8. Molecular docking

Structure-based *in silico* methods require the three-dimensional structures of protein and ligand molecules. These structures should be optimized and refined in terms of making them usable in computer-aided studies such as molecular docking and MD simulations. The 3D X-ray crystal structures of AChE and BuChE proteins were downloaded from Protein Data Bank (PDB codes 5EI5 and 5LKR, respectively). The structures were prepared for the ligand docking and further simulations via Protein Preparation module of Schrodinger's Maestro molecular modeling suite. The preparation process contains three main steps: pre-processing, optimization and minimization. First, the protein is pre-processed; bond orders are assigned and hydrogens are added. The disordered regions, missing loops and missing amino acid sidechains are also modelled and filled using the Prime module of Maestro in the pre-processing stage. Second, p*Ka* predictions and optimization are implemented at pH 7.4 using PROPKA. Third, energy minimization of the protein is performed using OPLS2005 (Optimized Potentials for Liquid Simulations 2005) force field. LigPrep module of Schrodinger's Maestro molecular modeling package is used for the preparation of the ligands. LigPrep uses Epik for proper assignments of

protonation states of selected molecules. It employs protonation and tautomerization state adjustment consistent with a specified pH range (in this study, pH value of 7.4 is considered). The molecular docking simulations were carried out using Glide/IFD (Sherman, Beard, & Farid, 2006) and quantum mechanics-polarized ligand docking (QPLD) (Cho, Guallar, Berne, & Friesner, 2005) approaches implemented into the Maestro molecular modeling package as well as MOE/IFD (Molecular Operating Environment, 2015) and GOLD (Verdonk, Cole, Hartshorn, Murray, & Taylor, 2003) docking programs. The IFD method provides flexibility to the binding pocket. The Glide/IFD consists of the following steps: (i) all the ligands were docked into the catalytic domain of the target using Glide/Standard Precision (SP) and then complexes with high docking scores were forwarded to next steps; (ii) amino acids of the complexes within 5 Å of the docked ligands were refined by Prime module of the Maestro; (iii) finally, all the ligands were redocked into the refined target via Glide/Extra Precision (XP) docking method. Two different docking scoring functions (London dG and Generalized-Born Volume Integral/Weighted Surface Area (GBVI/WSA) dG) were utilized in MOE/IFD docking. Triangle Matcher was chosen as the ligand placement methodology. MMFF94x force field is used to refine the free energy of binding in the second refinement step. 10 poses per each compound were generated in each re-scoring steps. In QPLD, initially, Glide/XP docking was carried out to generate 10 poses per docked compound. These poses were submitted to QM charge calculations which uses the 6-31G*/LACVP* basis set, B3LYP density functional and 'Ultrafine' SCF accuracy level. In GOLD algorithm, consensus docking protocol was used to generate protein–ligand complexes with GOLD software. The two docking scoring functions were combined (GoldScore and ChemScore). The following genetic algorithm parameters were used (population size, 50; selection pressure, 1.1; number of islands, 5; migrate, 10; mutate, 95; crossover, 95; niche size, 2; and number of operations, 107,000). Search efficiency was set to its maximum value (200%) exploring the search space as wide as possible in order to increase the reliability of the docking results.

4.9. MD simulations

All the MD simulations were carried out by Desmond code (Bowers et al., 2006). The interactions between the atoms were calculated by OPLS2005 force field. The particle-mesh Ewald method (Essmann et al., 1995) was implemented to calculate the long-range electrostatic interactions. The details of the MD simulations were described in our previous works (Rodrigues et al., 2018; Salmas, Seeman, Stein, & Durdagi, 2018).

4.10. Pharmacokinetic and toxicity predictions

Pharmacokinetic and toxicity predictions were investigated by MetaCore (version 2018), which is based on a high-quality, manually curated database of molecular interactions, molecular pathways, gene–disease associations, chemical metabolism and toxicity information. 26 different toxicity models such as cardiotoxicity, mutagenicity and cytotoxicity were predicted by 26 different toxicity QSAR models available under MetaCore. The quality of the derived models in MetaCore/MetaDrug is evaluated with specificity, sensitivity, accuracy and Matthews Correlation Coefficient (MCC).

Disclosure statement

No potential conflict of interest was reported by the authors.

Funding

This work was supported by the Bezmialem Research Fund of the Bezmialem Vakıf University [Project Number: 12.2015/28].

References

Alipour, M., Khoobi, M., Moradi, A., Nadri, H., Homayouni Moghadam, F., Emami, S., … Shafiee, A. (2014). Synthesis and anti-cholinesterase activity of new 7-hydroxycoumarin derivatives. *European Journal of Medicinal Chemistry*, *82*, 536–544. https://doi.org/10.1016/j.ejmech.2014.05.056

Ambure, P., Bhat, J., Puzyn, T., & Roy, K. (2018). Identifying natural compounds as multi-target-directed ligands against Alzheimer's disease: An *in silico* approach. *Journal of Biomolecular Structure and Dynamics*, 1–25. doi:10.1080/07391102.2018.1456975

Bowers, K., Chow, E., Xu, H., Dror, R., Eastwood, M., Gregersen, B., … Shaw, D. (2006). *Scalable algorithms for molecular dynamics simulations on commodity clusters*. Proceedings of the ACM/IEEE Conference on Supercomputing (SC06). Tampa: FL, November 11–17.

Cavdar, H., Senturk, M., Guney, M., Durdagi, S., Kayik, G., Supuran, C. T., & Ekinci, D. (2019). Inhibition of acetylcholinesterase and butyrylcholinesterase with uracil derivatives: Kinetic and computational studies. *Journal of Enzyme Inhibition and Medicinal Chemistry*, *34*(1), 429–437. doi:10.1080/14756366.2018.1543288

Chen, X., Murawski, A., Patel, K., Crespi, C. L., & Balimane, P. V. (2008). A novel design of artificial membrane for improving the PAMPA model. *Pharmaceutical Research*, *25*(7), 1511–1520. https://doi.org/10.1007/s11095-007-9517-8

Chen, Z., Digiacomo, M., Tu, Y., Gu, Q., Wang, S., Yang, X., … Pi, R. (2017). Discovery of novel rivastigmine-hydroxycinnamic acid hybrids as multi-targeted agents for Alzheimer's disease. *European Journal of Medicinal Chemistry*, *125*, 784–792. https://doi.org/10.1016/j.ejmech.2016.09.052

Chimichi, S., Boccalini, M., & Cosimelli, B. (2002). A new convenient route to 2-oxoethoxycoumarins: Key intermediates in the synthesis of natural products. *Tetrahedron*, *58*(24), 4851–4858. https://doi.org/10.1016/S0040-4020(02)00442-8

Cho, A. E., Guallar, V., Berne, B. J., & Friesner, R. (2005). Importance of accurate charges in molecular docking: Quantum mechanical/molecular mechanical (QM/MM) approach. *Journal of Computational Chemistry*, *26*(9), 915–931. doi:10.1002/jcc.20222

Dati, L. M., Ulrich, H., Real, C. C., Feng, Z. P., Sun, H. S., & Britto, L. R. (2017). Carvacrol promotes neuroprotection in the mouse hemiparkinsonian model. *Neuroscience*, *356*, 176–181. https://doi.org/10.1016/j.neuroscience.2017.05.013

Di, L., Kerns, E. H., Fan, K., McConnell, O. J., & Carter, G. T. (2003). High throughput artificial membrane permeability assay for blood–brain barrier. *European Journal of Medicinal Chemistry*, *38*(3), 223–232. https://doi.org/10.1016/S0223-5234(03)00012-6 doi:10.1016/S0223-5234(03)00012-6

Dutta, M., & Mattaparthi, V. S. K. (2018). *In silico* investigation on the inhibition of Aβ42 aggregation by Aβ40 peptide by potential of mean force study. *Journal of Biomolecular Structure and Dynamics*, *36*(3), 741–752. doi:10.1080/07391102.2017.1296783

Eghtedari, M. ,Sarrafi, Y., Nadri, H., Mahdavi, M., Moradi, A., Moghadam, F. H., Emami, S., Firoozpour, … Foroumadi, A. (2017). New tacrine-

derived AChE/BuChE inhibitors: Synthesis and biological evaluation of 5-amino-2-phenyl-4H-pyrano[2,3-b]quinoline-3- carboxylates. *European Journal of Medicinal Chemistry*, *128*, 237–246. https://doi.org/10.1016/j.ejmech.2017.01.042

Ellman, G. L., Courtney, K. D., Andres, V., & Featherstone, R. M. (1961). A new and rapid colorimetric determination of acetylcholinesterase activity. *Biochemical Pharmacology*, *7*(2), 88–90, INI, 91–95. https://doi.org/10.1016/0006-2952(61)90145-9

Essmann, U., Perera, L., Berkowitz, M. L., Darden, T., Lee, H., & Pedersen, L. G. (1995). A smooth particle mesh Ewald method. *The Journal of Chemical Physics*, *103*, 8577. https://doi.org/10.1063/1.470117

Estrada, M., Herrera-Arozamena, C., Pérez, C., Viña, D., Romero, A., Morales-García, J. A., … Rodríguez-Franco, M. I. (2016). New cinnamic - *N*-benzylpiperidine and cinnamic - *N,N*-dibenzyl(*N*-methyl)amine hybrids as Alzheimer-directed multitarget drugs with antioxidant, cholinergic, neuroprotective and neurogenic properties. *European Journal of Medicinal Chemistry*, *121*, 376–386. https://doi.org/10.1016/j.ejmech.2016.05.055

Ferreira Neto, D. C., Alencar Lima, J., Sobreiro Francisco Diz de Almeida, J., Costa França, T. C., Jorge do Nascimento, C., & Figueroa Villar, J. D. (2018). New semicarbazones as gorge-spanning ligands of acetylcholinesterase and potential new drugs against Alzheimer's disease: Synthesis, molecular modeling, NMR, and biological evaluation. *Journal of Biomolecular Structure and Dynamics*, *36*(15), 4099–4113. doi:10.1080/07391102.2017.1407676

Gao, X.-H., Tang, J.-J., Liu, H.-R., & Liu, L.-B, Liu, Y.-Z. (2019). Structure–activity study of fluorine or chlorine-substituted cinnamic acid derivatives with tertiary amine side chain in acetylcholinesterase and butyrylcholinesterase inhibition. *Drug Development Research*. doi: 10.1002/ddr.21515

Guzior, N., Bajda, M., Rakoczy, J., Brus, B., Gobec, S., & Malawska, B. (2015). Isoindoline-1,3-dione derivatives targeting cholinesterases: Design, synthesis and biological evaluation of potential anti-Alzheimer's agents. *Bioorganic and Medicinal Chemistry*, *23*(7), 1629–1637. https://doi.org/10.1016/j.bmc.2015.01.045

Guzior, N., Bajda, M., Skrok, M., Kurpiewska, K., LewiÅski, K., Brus, B., … Malawska, B. (2015). Development of multifunctional, heterodimeric isoindoline-1,3-dione derivatives as cholinesterase and β-amyloid aggregation inhibitors with neuroprotective properties. *European Journal of Medicinal Chemistry*, *92*, 738–749. https://doi.org/10.1016/j.ejmech.2015.01.027

Höferl, M., Buchbauer, G., Jirovetz, L., Schmidt, E., Stoyanova, A., Denkova, Z., … Geissler, M. (2009). Correlation of antimicrobial activities of various essential oils and their main aromatic volatile constituents. *Journal of Essential Oil Research*, *21*(5), 459–463. https://doi.org/10.1080/10412905.2009.9700218

Hussein, J., El-Banna, M., Mahmoud, K. F., Morsy, S., Abdel Latif, Y., Medhat, D., … El-Daly, S. M. (2017). The therapeutic effect of nano-encapsulated and nano-emulsion forms of carvacrol on experimental liver fibrosis. *Biomedicine and Pharmacotherapy*, *90*, 880–887. https://doi.org/10.1016/j.biopha.2017.04.020

Iqbal, S., Anantha Krishnan, D., & Gunasekaran, K. (2018). Identification of potential PKC inhibitors through pharmacophore designing, 3D-QSAR and molecular dynamics simulations targeting Alzheimer's disease. *Journal of Biomolecular Structure and Dynamics*, *36*(15), 4029–4044. doi:10.1080/07391102.2017.1406824

Kurt, B. Z., Gazioglu, I., Sonmez, F., & Kucukislamoglu, M. (2015). Synthesis, antioxidant and anticholinesterase activities of novel coumarylthiazole derivatives. *Bioorganic Chemistry*, *59*, 80–90. https://doi.org/10.1016/j.bioorg.2015.02.002

Kurt, B. Z., Gazioglu, I., Dag, A., Salmas, R. E., Kayik, G., Durdagi, S., & Sonmez, F. (2017). Synthesis, anticholinesterase activity and molecular modeling study of novel carbamate-substituted thymol/carvacrol derivatives, *Bioorganic & Medicinal Chemistry*, *25*(4), 1352–1363. https://doi.org/10.1016/j.bmc.2016.12.037

León, R., Garcia, A. G., & Marco-Contelles, J. (2013). Recent advances in the multitarget-directed ligands approach for the treatment of Alzheimer's disease. *Medicinal Research Reviews*, *33*(1), 139–189. https://doi.org/10.1002/med.20248

Li, Y., Qiang, X., Luo, L., Yang, X., Xiao, G., Liu, Q., … Deng, Y. (2017). Aurone Mannich base derivatives as promising multifunctional agents with acetylcholinesterase inhibition, anti-β-amyloid aggregation and neuroprotective properties for the treatment of Alzheimer's disease. *European Journal of Medicinal Chemistry*, *126*, 762–775. https://doi.org/10.1016/j.ejmech.2016.12.009

Liu, Z., Fang, L., Zhang, H., Gou, S., & Chen, L. (2017). Design, synthesis and biological evaluation of multifunctional tacrine-curcumin hybrids as new cholinesterase inhibitors with metal ions-chelating and neuroprotective property. *Bioorganic and Medicinal Chemistry*, *25*(8), 2387–2398. https://doi.org/10.1016/j.bmc.2017.02.049

López, M. D., Campoy, F. J., Pascual-Villalobos, M. J., Muñoz-Delgado, E., & Vidal, C. J. (2015). Acetylcholinesterase activity of electric eel is increased or decreased by selected monoterpenoids and phenylpropanoids in a concentration-dependent manner. *Chemico-Biological Interactions*, *229*, 36–43. https://doi.org/10.1016/j.cbi.2015.01.006

Majdi, M., Malekzadeh-Mashhady, A., Maroufi, A., & Crocoll, C. (2017). Tissue-specific gene-expression patterns of genes associated with thymol/carvacrol biosynthesis in thyme (*Thymus vulgaris L.*) and their differential changes upon treatment with abiotic elicitors. *Plant Physiology and Biochemistry, 115*, 152–162.2017.03.016 doi:10.1016/j.plaphy

Maryamabadi, A., Hasaninejad, A., Nowrouzi, N., & Mohebbi, G. (2017). Green synthesis of novel spiro-indenoquinoxaline derivatives and their cholinesterases inhibition activity. *Bioorganic and Medicinal Chemistry*, *25*(7), 2057–2064.https://doi.org/10.1016/j.bmc.2017.02.017

MetaCore/MetaDrug Comprehensive Systems Biology Analysis Suite. (2018). Philadelphia, PA: Clarivate Analytics. https://portal.genego.com/

Mohamed, T., Osman, W., Tin, G., & Rao, P. P. N. (2013). Selective inhibition of human acetylcholinesterase by xanthine derivatives: *In vitro* inhibition and molecular modeling investigations. *Bioorganic & Medicinal Chemistry Letters*, *23*(15), 4336–4341. https://doi.org/10.1016/j.bmcl.2013.05.092

Molecular Operating Environment. (2015). Montreal, QC: Chemical Computing Group.

Muñoz-Ruiz, P., Rubio, L., García-Palomero, E., Dorronsoro, I., Del Monte-Millán, M., Valenzuela, R., … Martínez, A. (2005). Design, synthesis, and biological evaluation of dual binding site acetylcholinesterase inhibitors: New disease-modifying agents for Alzheimer's disease. *Journal of Medicinal Chemistry*, *48*(23), 7223–7233. https://doi.org/10.1021/jm0503289

Nepovimova, E., Korabecny, J., Dolezal, R., Babkova, K., Ondrejicek, A., Jun, D., … Kuca, K. (2015). Tacrine–trolox hybrids: A novel class of centrally active, nonhepatotoxic multi-target-directed ligands exerting anticholinesterase and antioxidant activities with low *in vivo* toxicity. *Journal of Medicinal Chemistry*, *58*(22), 8985–9003. https://doi.org/10.1021/acs.jmedchem.5b01325

Panek, D., Więckowska, A., Wichur, T., Bajda, M., Godyń, J., Jończyk, J., … Malawska, B. (2017). Design, synthesis and biological evaluation of new phthalimide and saccharin derivatives with alicyclic amines targeting cholinesterases, beta-secretase and amyloid beta aggregation. *European Journal of Medicinal Chemistry*, *125*, 676–695. https://doi.org/10.1016/j.ejmech.2016.09.078

Pérez-Areales, F. J., D., Pietro, O., Espargaró, A., Vallverdú-Queralt, A., Galdeano, C., Ragusa, I. M., …., Muñoz-Torrero, D. (2014). Shogaol–huprine hybrids: Dual antioxidant and anticholinesterase agents with β-amyloid and tau anti-aggregating properties. *Bioorganic and Medicinal Chemistry*, *22*(19), 5298–5307. https://doi.org/10.1016/j.bmc.2014.07.053

Pascoini, A. L., Federico, L. B., Arêas, A. L. F., Verde, B. A., Freitas, P. G., & Camps, I. (2019). In silico development of new acetylcholinesterase inhibitors. *Journal of Biomolecular Structure and Dynamics*, *37*(4), 1007–1021. doi:10.1080/07391102.2018.1447513

Rodrigues, M. J., Slusarczyk, S., Pecio, Ł., Matkowski, A., Salmas, R. E., Durdagi, S., …., Custódio, L. (2018). *In vitro* and *in silico* approaches to appraise *Polygonum maritimum* L. as a source of innovative products with anti-ageing potential. *Industrial Crops and Products*, *111*, 391–399. https://doi.org/10.1016/j.indcrop.2017.10.046

Rodríguez, J., Ortuño, C., Benedito, J., & Bon, J. (2013). Optimization of the antioxidant capacity of thyme (*Thymus vulgaris* L.) extracts: Management of the Drying Process. *Industrial Crops and Products*, *46*, 258–263. https://doi.org/10.1016/j.indcrop.2013.02.002

Sağlık, B. N., Ilgın, S., & Özkay, Y. (2016). Synthesis of new donepezil analogues and investigation of their effects on cholinesterase enzymes. *European Journal of Medicinal Chemistry*, *124*, 1026–1040. https://doi.org/10.1016/j.ejmech.2016.10.042

Salmas, R. E., Seeman, P., Stein, M., & Durdagi, S. (2018). Structural investigation of the dopamine-2 receptor agonist bromocriptine binding to dimeric D2HighR and D2LowR states. *Journal of Chemical Information and Modeling*, *58*(4), 826–836. https://doi.org/10.1021/acs.jcim.7b00722

Sherman, W., Beard, H. S., & Farid, R. (2006). Use of an induced fit receptor structure in virtual screening. *Chemical Biology and Drug Design*, *67*(1), 83–84. https://doi.org/10.1111/j.1747-0285.2005.00327.x

Shiri, F., Pirhadi, S., & Ghasemi, J. B. (2018). Dynamic structure based pharmacophore modeling of the Acetylcholinesterase reveals several potential inhibitors. *Journal of Biomolecular Structure and Dynamics*, 1–13. doi:10.1080/07391102.2018.1468281

Sonmez, F., Zengin Kurt, B., Gazioglu, I., Basile, L., Dag, A., Cappello, V., … Guccione, S. (2017). Design, synthesis and docking study of novel coumarin ligands as potential selective acetylcholinesterase inhibitors. *Journal of Enzyme Inhibition and Medicinal Chemistry*, *32*(1), 285–297. https://doi.org/10.1080/14756366.2016.1250753

Sow, L. C., Tirtawinata, F., Yang, H., Shao, Q., & Wang, S. (2017). Carvacrol nanoemulsion combined with acid electrolysed water to inactivate bacteria, yeast *in vitro* and native microflora on shredded cabbages. *Food Control*, *76*, 88–95. https://doi.org/10.1016/j.foodcont.2017.01.007

Tommonaro, G., García-Font, N., Vitale, R. M., Pejin, B., Iodice, C., Cañadas, S., … Oset-Gasque, M. J. (2016). Avarol derivatives as competitive AChE inhibitors, non hepatotoxic and neuroprotective agents for Alzheimer's disease. *European Journal of Medicinal Chemistry*, *122*, 326–338. https://doi.org/10.1016/j.ejmech.2016.06.036

Verdonk, M. L., Cole, J. C., Hartshorn, M. J., Murray, C. W., & Taylor, R. D. (2003). Improved protein–ligand docking using GOLD. *Proteins: Structure, Function and Genetics*, *52*, 609–623. https://doi.org/10.1002/prot.10465

Wang, L., Wang, Y., Tian, Y., Shang, J., Sun, X., Chen, H., … Tan, W. (2017). Design, synthesis, biological evaluation, and molecular modeling studies of chalcone-rivastigmine hybrids as cholinesterase inhibitors. *Bioorganic and Medicinal Chemistry*, *25* (1), 360–371. https://doi.org/10.1016/j.bmc.2016.11.002

Wang, X. Q., Xia, C. L., S. Bin, Tan, J. H, C., Ou, T. M., Huang, S. L., … Huang, Z. S. (2014). Design, synthesis, and biological evaluation of 2-arylethenylquinoline derivatives as multifunctional agents for the treatment of Alzheimer's disease. *European Journal of Medicinal Chemistry*, *89*, 349–361. https://doi.org/10.1016/j.ejmech.2014.10.018

Wu, J., Tian, Y., Wang, S., Pistolozzi, M., Jin, Y., Zhou, T., … Tan, W. (2017). Design, synthesis and biological evaluation of bambuterol analogues as novel inhibitors of butyrylcholinesterase. *European Journal of Medicinal Chemistry*, *126*, 61–71. https://doi.org/10.1016/j.ejmech.2016.08.061 doi:10.1016/j.ejmech.2016.08.061

Xia, C. L., Wang, N., Guo, Q. L., Liu, Z. Q., Wu, J. Q., Huang, S. L., … Huang, Z. S. (2017). Design, synthesis and evaluation of 2-arylethenyl-*N*-methylquinolinium derivatives as effective multifunctional agents for Alzheimer's disease treatment. *European Journal of Medicinal Chemistry*, *130*, 139–153. https://doi.org/10.1016/j.ejmech.2017.02.042

Zhong, Z., Wang, B., Dai, M., Sun, Y., Sun, Q., Yang, G., & Bian, L. (2013). Carvacrol alleviates cerebral edema by modulating AQP4 expression after intracerebral hemorrhage in mice. *Neuroscience Letters*, *555, 24–29.* https://doi.org/10.1016/j.neulet.2013.09.023

Zilbeyaz, K., Stellenboom, N., Güney, M., Oztekin, A., & Senturk, M. (2018). Effects of aryl methanesulfonate derivatives on acetylcholinesterase and butyrylcholinesterase. *Journal of Biochemical and Molecular Toxicology*, *32*(11), e22210. doi:10.1002/jbt.22210